Ordering of two-dimensional crystals confined in strips of finite width

A. Ricci,[1] P. Nielaba,[2] S. Sengupta,[3] and K. Binder[1]
[1]*Institut für Physik, Johannes Gutenberg-Universität Mainz, D-55099 Mainz, Staudinger Weg 7, Germany*
[2]*Physics Department, University of Konstanz, D-78457 Konstanz, Germany*
[3]*Unit for Nanoscience and Technology, S. N. Bose National Centre for Basic Sciences, Block JD, Sector III, Salt Lake, Calcutta 700098, India*
(Received 27 July 2006; published 18 January 2007)

Monte Carlo simulations are used to study the effect of confinement on a crystal of point particles interacting with an inverse power law potential $\propto r^{-12}$ in $d=2$ dimensions. This system can describe colloidal particles at the air-water interface, a model system for experimental study of two-dimensional melting. It is shown that the state of the system (a strip of width D) depends very sensitively on the precise boundary conditions at the two "walls" providing the confinement. If one uses a corrugated boundary commensurate with the order of the bulk triangular crystalline structure, both orientational order and positional order is enhanced, and such surface-induced order persists near the boundaries also at temperatures where the system in the bulk is in its fluid state. However, using smooth repulsive boundaries as walls providing the confinement, only the orientational order is enhanced, but positional (quasi-)long range order is destroyed: The mean-square displacement of two particles n lattice parameters apart in the y direction along the walls then crosses over from the logarithmic increase (characteristic for $d=2$) to a linear increase with n (characteristic for $d=1$). The strip then exhibits a vanishing shear modulus. These results are interpreted in terms of a phenomenological harmonic theory. Also the effect of incommensurability of the strip width D with the triangular lattice structure is discussed, and a comparison with surface effects on phase transitions in simple Ising and XY models is made.

DOI: 10.1103/PhysRevE.75.011405 PACS number(s): 82.70.Dd, 0.5.10.Ln, 68.55.−a, 64.60.Cn

I. INTRODUCTION

Nanotechnology is promising to yield a new generation of materials and devices, a basic approach being the assembly of nanoparticles into spatially extended regular structures. In this context, colloidal crystals are a valuable model system, since the effective interactions between colloidal particles can be manipulated to a large extent, and convenient techniques to observe the structure and dynamics of such systems are available [1–4]. Colloidal dispersions under geometric confinement then can serve to help understand the effects of confinement on the ordering of various types of nanoparticles.

Related phenomena occur in a wide variety of systems, e.g., electrons at the surface of liquid helium that is confined in a quasi-one-dimensional channel [5] example for a confined Wigner crystal [6]; another such system where particles occur under geometric confinement are "dusty plasmas" [7] (e.g., negatively charged SiO_2 fine particles with 10 μm diameter are suspended in weakly ionized rf Ar discharges [8]); hard disks [9,10] and magnetorheological (MR) colloids under confinement [11,12] are of great interest for various microfluidic and other applications. In the present paper, we shall not address specific systems or applications, but rather we are concerned with the generic effect of confinement on crystalline order in $d=2$ dimensions, paying attention to the extent and range over which the confining boundaries disturb (or enhance, respectively) the degree of order.

The effect of external walls (and/or free surfaces, respectively) on phase behavior has been studied for a long time [13–22]. To set the scene, we briefly recall the simplest case, a system undergoing a second-order phase transition in the bulk from a disordered state to an ordered state with a one-component order parameter (e.g., an Ising ferromagnet, Fig. 1). One must distinguish between boundary conditions at the wall providing a linear coupling to the order parameter ("surface magnetic field" H_1 in the case of a ferromagnet) and a quadratic coupling (as it occurs in ferromagnets where missing neighbors imply that the spins in the surface plane experience less exchange interactions to neighboring spins than the spins in the bulk). In both cases the range over which the order near the surface is either enhanced or reduced is of the order of the correlation length ξ_b of order parameter fluctuations in the bulk. At the critical temperature T_c of the second order transition where ξ_b has diverged to infinity, the exponential decay towards the bulk has been replaced by a power-law behavior [Fig. 1(b)]. Note that in Fig. 1 we have only considered the case that the field H_1 at the surface acts in the same direction as the order parameter Ψ_b in the bulk [Fig. 1(c)]. The case that the field at the surface acts in the direction opposite to the order parameter in the bulk is also of great interest, it may lead to the formation of (ideally macroscopically thick) "wetting layers" [14–19], but this phenomenon is not under consideration here.

Figure 1 is not the whole story, of course, since at a phase transition it is also of interest to consider the correlation function $G(\vec{r}_1,\vec{r}_2)=\langle\Psi(\vec{r}_1)\Psi(\vec{r}_2)\rangle$ of the local order parameter $\Psi(\vec{r})=\Psi(\vec{\rho},z)$, $\vec{\rho}$ being the set of $(d-1)$-dimensional coordinates parallel to the surface. Since translational invariance is only broken in the z direction normal to the wall, we can choose $\vec{\rho}_1=0$, $\vec{\rho}_2=\vec{\rho}$, to redefine the correlation function as $G(\vec{r}_1,\vec{r}_2)\equiv g(\vec{\rho},z_1,z_2)$. While it turns out [13–15] that the decay of g for $T>T_c$ is always given by an exponential decay, $g\propto\exp(-|\vec{r}_1-\vec{r}_2|/\xi_b)$ and for $T\to T_c$ the decay length ξ_b does not depend on the direction of $\vec{r}_1-\vec{r}_2$, the power law at T_c does depend on the direction,

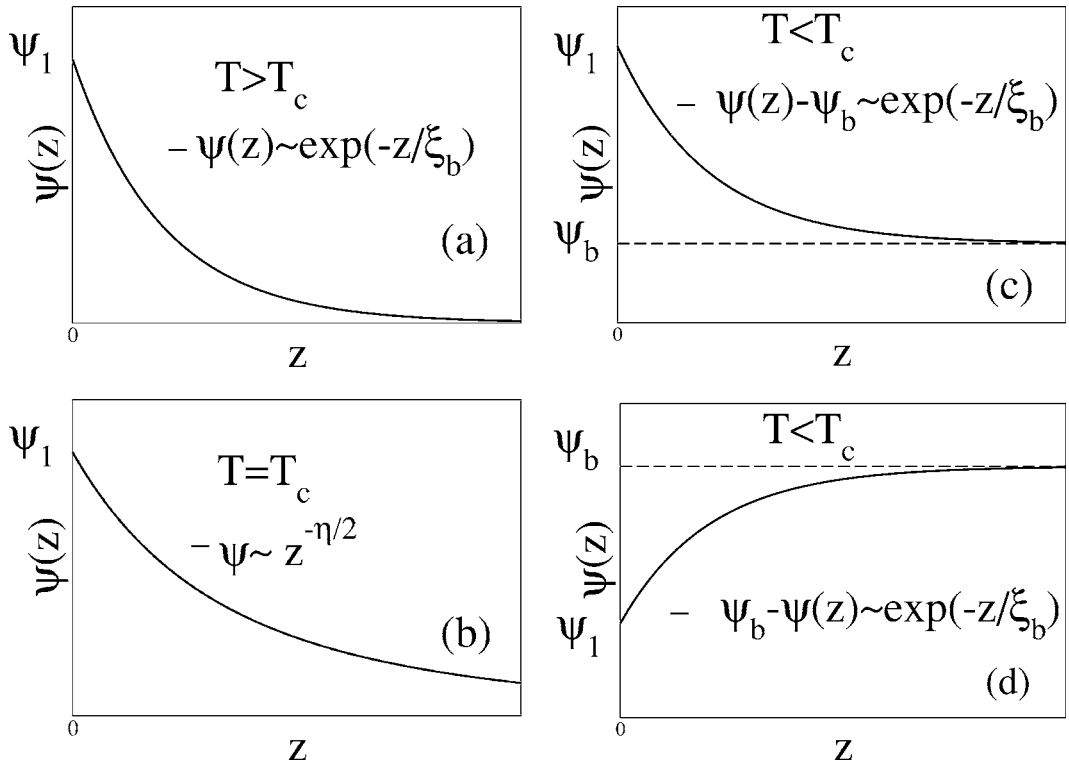

FIG. 1. Schematic variation of the local order parameter $\Psi(z)$ as a function of the distance z from a wall (or free surface, respectively) that is located at $z=0$. The second order phase transition from the disordered phase (with order parameter $\Psi_b=0$ in the bulk) to the ordered phase (where $\Psi_b>0$) occurs at T_c in the bulk. In cases (a)–(c) it is assumed that at the wall at $z=0$ a local surface field $H(z)=H_1\delta(z)$ conjugate to the order parameter $\Psi(z)$ acts. As a result, there exists not only a local order parameter Ψ_1 right at the surface, but surface-induced order occurs in a region of a width of order ξ_b, the order-parameter correlation length in the bulk, both for $T>T_c$ and for $T<T_c$. This surface induced order decays to zero for $T>T_c$ and to Ψ_b for $T<T_c$. Right at $T=T_c$ the order decays also to zero, but much more slowly namely according to a power law, with an exponent that has been denoted as $\eta/2$ here. In case (d) it is assumed that the surface is "neutral," no sign of the order parameter is preferred, and so the surface couples only to the order parameter square: the most frequent case then is that the ordering tendency at the surface is reduced (e.g., by the "missing neighbor effect"). Then $\Psi_1<\Psi_b$ for $T<T_c$, and $\Psi(z)$ relaxes towards Ψ_b from below. The range over which Ψ_b and $\Psi(z)$ appreciably differ is again of the order of ξ_b.

$$g(\vec{\rho},z_1,z_2) \propto \rho^{-(d-2+\eta_\parallel)},z_1, \quad z_2 \text{ finite}, \quad \rho \to \infty, \tag{1}$$

$$g(\vec{\rho},z_1,z_2) \propto |z_2 - z_1|^{-(d-2+\eta_\perp)}, \quad |\rho|, \quad z_1 \text{ finite}, \quad z_2 \to \infty. \tag{2}$$

The exponents $\eta_\parallel, \eta_\perp$ differ also from the exponent encountered in the bulk, $G(\vec{r}_1,\vec{r}_2) \propto |\vec{r}_2 - \vec{r}_1|^{-(d-2+\eta)}$.

All the above results apply only for a semi-infinite geometry, and it is also of interest to ask what happens when one considers instead a thin film of a large but finite thickness D. Then the correlation length can grow towards infinity only in the $(d-1)$ directions parallel to the confining walls. As a result, a crossover from d-dimensional critical behavior to $(d-1)$-dimensional critical behavior sets in at a temperature near T_c when ξ_b has grown to about the distance D between the walls. At a (shifted) transition temperature $T_c(D)$, a second order transition with $(d-1)$-dimensional critical behavior occurs, if $d>2$. In the case $d=2$, however, $T_c(D)=0$, since $d-1=1$ then coincides with the lower critical dimension. The correlation length $\xi(T)$ grows as $\xi(T) \propto [T - T_c(\infty)]^{-\nu}$ (with $\nu=1$ [23]) until $\xi(T)$ becomes of the order of D, and then a crossover sets in to a behavior [24] $\xi(T) \propto D \exp[(\sigma/k_BT)D]$, σ being the interfacial tension between coexisting phases in $d=2$. Note that for the XY model, however, $d=2$ is the lower critical dimension [25–29], and then $\xi(T)$ grows as $\xi(T) \propto \exp\{\text{const}[T-T_c(\infty)]^{-1/2}\}$ until $\xi(T)$ becomes of the order of D, and then a crossover sets in to [30]

$$\xi(T) = 2\Gamma(T)D/k_BT = D/[\pi\eta(T)], \tag{3}$$

$\Gamma(T)$ being the helicity modulus of the $d=2$ bulk XY model, and $\eta(T)$ describes the decay of the spin-spin correlation function of the XY model in $d=2$ at all temperatures in the low-temperature phase (recall that $\Psi_b \equiv 0$ in this model).

As a result, subtle crossovers occur in the correlation functions in thin films near the critical point T_c of the bulk system (and below it). In an Ising system, Eq. (1) is expected to hold near T_c only for $\rho<\xi(T) \propto D$, while for $\rho>\xi(T)$ an exponential decay proportional to $\exp[-\rho/\xi(T)]$ occurs. For $T<T_c$, we have $g \approx \Psi_b^2$ for $\rho<\xi(T)$, while for $\rho>\xi(T)$ the same exponential decay occurs [but now $\xi(T)$ can be extremely large, due to the exponential dependence of $\xi(T)$ on D, as noted above]. In the XY model, however, we expect a power law decay of g with ρ for $\rho<D$ for all temperatures

below T_c, and for $\rho > D$ an exponential decay $\exp[-\rho/\xi(T)]$ with $\xi(T)$ being given by Eq. (3) takes over.

We have emphasized here the behavior of the $d=2$ XY model, since there are very close analogies between the ordering of that model and the behavior of positional order in $d=2$ crystals. In the next section, we shall briefly review the theoretical predictions on (harmonic) crystals in $d=1$ and $d=2$ dimensions and recall the theoretical predictions on two-dimensional melting that are most relevant in the present context. We then discuss how the above scenario on surface and size effects in the strip geometry can be carried over to this problem qualitatively.

II. CRYSTALLINE ORDER IN LOW DIMENSION: THEORETICAL BACKGROUND

As is well known, in systems with short range potentials crystalline order in $d=1$ dimension is possible at $T=0$ only, and hence the system at any nonzero temperature is molten into a fluid structure [31,32].

A simple model of this situation is provided by the Hamiltonian of a harmonic chain [31]

$$\mathcal{H} = \frac{1}{2}\sum_{\ell} [\pi_\ell^2/m + mc^2(y_{\ell+1} - y_\ell - a)^2/a^2], \tag{4}$$

where point particles of mass m have positions y_ℓ and conjugate momenta π_ℓ. In the classical ground state one has $y_n = y_0 + na$, $n = 1, 2, \ldots, N \to \infty$, a being the lattice spacing of the one-dimensional periodic lattice appearing in the ground state. The parameter c plays the role of a sound velocity when one determines the eigenfrequencies of $\mathcal{H}$ ($\omega = cq$ for wave numbers $q \to 0$). From Eq. (4) it is straightforward to calculate the correlation function of the mean square displacements $u_n = y_n - na$ as

$$\langle (u_n - u_0)^2 \rangle = na^2 k_B T/(mc^2) = n\delta^2. \tag{5}$$

Here δ characterizes the local displacement. The obvious interpretation of Eq. (5) is that the relative displacements $u_\ell - u_{\ell-1}$ at each index ℓ of the one-dimensional (1D) lattice add up in a random-walk-like fashion. The static structure factor

$$S(q) = \frac{1}{N}\sum_{\ell,\ell'} \langle \exp[iq(y_\ell - y_{\ell'})] \rangle \tag{6}$$

for this harmonic crystal can be expressed in terms of the mean-square displacements as

$$S(q) = \frac{1}{N}\sum_{\ell,\ell'} \exp[iq(\ell - \ell')a] \exp\left(-\frac{1}{2} q^2 \langle (u_\ell - u_{\ell'})^2 \rangle \right). \tag{7}$$

Using then Eq. (5) in Eq. (7) it is straightforward to show that [31]

$$S(q) = \sinh(q^2\delta^2/2)/[\cosh(q^2\delta^2/2) - \cos(qa)]. \tag{8}$$

Since $\cos(qa) = 1$ for the Bragg peak positions $q_\nu a = 2\pi\nu$, $\nu = 0, \pm 1, \pm 2, \ldots$, one recognizes that for small δ the structure factor has a series of rather sharp peaks at the Bragg positions, which smoothly develop towards a series of delta functions $\delta(q - q_\nu)$ as $\delta \to 0$ [which means $T \to 0$, cf. Eq. (5)]. For T small but nonzero, on the other hand, the structure factor resembles a series of Lorentzian peaks,

$$S(q \approx q_\nu) \approx q_\nu^2 \delta^2/[q_\nu^4 \delta^4/4 + (q - q_\nu)^2 a^2] = (4/q_\nu^2\delta^2)[1 + (q - q_\nu)^2 \nu^{-4} \xi^2]^{-1}$$

$$\nu = 1, 2, 3, \ldots, \quad \xi = amc^2/(2\pi^2 k_B T). \tag{9}$$

The length ξ describing the inverse width of the first pseudo-Bragg peak can be interpreted as the correlation length of positional order in the 1D chain. From Eq. (5) we recognize that this corresponds to a distance na along the chain for which the mean-square displacement has grown to a value $1/(2\pi^2)$, which hence is an analog to the "Lindemann criterion" of melting familiar from crystals in $d=3$ [33]. Note that Piacente *et al.* [6] suggested to generalize the "Lindemann criterion" to estimate the melting temperature of a crystal to low-dimensional systems by requiring that the "Lindemann parameter" $L_p = \langle (u_1 - u_0)^2 \rangle / a^2 = 0.1$. Such a notion would imply that even a crystal in $d=1$ has a nonzero melting temperature $T_m > 0$, as Eq. (5) shows. Equation (9) shows this makes little sense, however ($\xi/a \approx 1/2$ at this temperature T_m). As is well known, Eqs. (8) and (9), do provide a realistic description of materials such as the mercury chain compound $Hg_{3-\delta}AsF_6$ [31,32].

We now turn to the two-dimensional case. Being interested in point particles that interact with pairwise potentials $V(r)$ depending only on the absolute value r of their distance, the relevant crystal structure is the triangular lattice. In $d=2$, however, we now must consider both positional order and bond orientational order [19,27,34–39].

The average positional long range order can be studied most conveniently by studying the order parameter components, see Fig. 2,

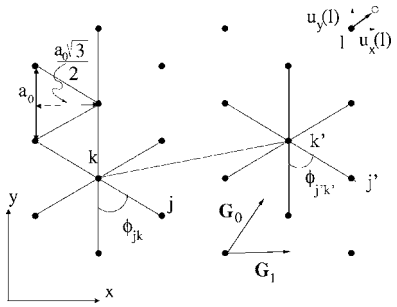

FIG. 2. Geometry of the triangular lattice: the y axis is oriented along a nearest neighbor direction, the x axis perpendicular to it. The lattice spacing is denoted as a_0, and hence neighboring rows of particles along the y axis are at distance $a_0\sqrt{3}/2$. The angle between a bond connecting particles k and j and a reference direction (the y direction in the figure) is denoted as ϕ_{jk}. The basic vectors of the reciprocal lattice are denoted as $\vec{G}_0$ and $\vec{G}_1$. The displacement $\vec{u}(\ell)$ of the ℓth particle from its ideal lattice position is decomposed in its Cartesian coordinates $u_x(\ell)$ and $u_y(\ell)$.

$$\Psi_{\vec{G}_0} = \frac{1}{N}\left|\sum_{\ell=1}^{N} \exp[i\vec{G}_0 \cdot \vec{r}_\ell|]\right|,$$

$$\Psi_{\vec{G}_1} = \frac{1}{N}\left|\sum_{\ell=1}^{N} \exp[i\vec{G}_1 \cdot \vec{r}_\ell]\right|, \tag{10}$$

where $\vec{r}_\ell$ is the position of the lth particle and $\vec{G}_0, \vec{G}_1$ are the two basic vectors of the reciprocal lattice. From the simulation, the full distribution function $P(\Psi_{\vec{G}_0}, \Psi_{\vec{G}_1})$ is accessible. Note that the static structure factor

$$S(\vec{q}) = \frac{1}{N}\sum_{\ell,\ell'} \langle \exp[i\vec{q} \cdot (\vec{r}_\ell - \vec{r}_{\ell'})]\rangle \tag{11}$$

has peaks at the reciprocal lattice spots, and the maximum values of $S(\vec{q})$ at these peak positions are simply related to the second moment of the order parameter distribution, e.g.,

$$S(\vec{G}_0) = N\langle \Psi^2_{\vec{G}_0}\rangle, \quad S(\vec{G}_1) = N\langle \Psi^2_{\vec{G}_1}\rangle. \tag{12}$$

The local orientational order parameter Ψ_k is defined as [33–39] (see Fig. 2)

$$\Psi_6(k) = \frac{1}{6}\sum_{j(\text{n.n.of } k)} \exp(6i\phi_{jk}), \tag{13}$$

where the 6 in the argument of the exponential function expresses the fact that in the ideal triangular structure the angles ϕ_{jk}'s of a considered particle can differ only by multiples of $2\pi/6$. The average orientational order parameter $\bar{\Psi}_6$ and its correlation function $g_6(\vec{r})$ then become

$$\bar{\Psi}_6 = \frac{1}{N}\left\langle \left|\sum_{\ell=1}^{N} \Psi_6(\ell)\right| \right\rangle, \quad g_6(\vec{r}) = \langle |\Psi_6(k)\Psi_6(k')|\rangle, \tag{14}$$

where $\vec{r} = \vec{r}_k - \vec{r}_{k'}$. Note that $g_6(\vec{r}\to\infty) = \bar{\Psi}_6^2$ if orientational long range order exists.

Again it is of interest to consider the predictions of the harmonic approximation. We start from the continuum approximation for a two-dimensional elastic solid that has a triangular lattice structure [33]

$$\mathcal{H}_{e\ell} = \frac{1}{2}\int \frac{dQ_x}{2\pi}\int \frac{dQ_y}{2\pi}[(\lambda + 2\mu - p)Q^2 u_L^2 + (\mu - p)Q^2 u_T^2]. \tag{15}$$

Here the integration is extended over the first Brillouin zone, λ and μ are the well-known Lame coefficients, and p is the hydrostatic pressure. The Fourier transform $\vec{u}(\vec{Q})$ of the displacement vector $\vec{u}(\ell)$ [cf. Fig. 2] has been decomposed into longitudinal (L) and transverse (T) components,

$$\vec{u}(\ell) = (1/\sqrt{N})\sum_{\vec{Q}} \vec{u}(\vec{Q})\exp[i\vec{Q} \cdot \vec{r}_\ell], \quad u_L(\vec{Q}) = \hat{\vec{Q}} \cdot \vec{u}(\vec{Q}),$$

$$\vec{u}_T(\vec{Q}) = \vec{u}(\vec{Q}) - \hat{\vec{Q}}u_L(\vec{Q}), \quad \hat{\vec{Q}} \equiv \vec{Q}/|\vec{Q}|. \tag{16}$$

A quantity of basic interest that we wish to calculate from the elastic Hamiltonian, Eq. (15), is the displacement correlation function

$$G(\vec{r}) \equiv \langle[\vec{u}(\vec{r}) - \vec{u}(0)]^2\rangle = (2/N)\sum_{\vec{Q}} \langle|\vec{u}(\vec{Q})|^2\rangle[1 - \cos(\vec{Q} \cdot \vec{r})]. \tag{17}$$

Note that $G(\vec{r})$ also controls the static structure factor $S(\vec{q})$ [Eq. (11)] since ($\vec{r}_\ell = \vec{R}_\ell + \vec{u}_\ell, \vec{R}_\ell$ = reference reference position in the perfect triangular lattice)

$$S(\vec{q}) = \frac{1}{N}\sum_{\ell,\ell'} \exp[i\vec{q} \cdot (\vec{R}_\ell - \vec{R}_{\ell'})]\exp\left(-\frac{1}{2}\langle[\vec{q} \cdot (\vec{u}_\ell - \vec{u}_{\ell'})]^2\rangle\right). \tag{18}$$

Using the equipartition theorem one readily shows from Eq. (15) that [33]

$$\langle u_\alpha(\vec{Q})u_\beta(-\vec{Q})\rangle = \frac{k_B T/Q^2}{(\lambda + 2\mu - p)}\hat{Q}_\alpha\hat{Q}_\beta + \frac{k_B T/Q^2}{\mu - p}(\delta_{\alpha\beta} - \hat{Q}_\alpha\hat{Q}_\beta), \tag{19}$$

where α, β denote Cartesian components. Here we shall focus in particular on the displacement correlation of y components and consider also a distance $\vec{r}$ along the y direction, to find

$$\langle[u_y(na_0) - u_y(0)]^2\rangle = \frac{2}{N}\sum_{Qx}\sum_{Qy}\langle u_y(\vec{Q})u_y(-\vec{Q})\rangle \times[1 - \cos(Q_y n a_0)], \tag{20}$$

where the values Q_x, Q_y over which the sums are extended are determined by the geometry of the considered crystal, and the boundary conditions chosen. We here consider a lattice of size D in the x direction and size L in the y direction, and choose periodic boundary conditions. It is convenient to measure the lengths in the y direction in units of the lattice spacing $a_0 \equiv 1$ (Fig. 2) and in the y direction in units of $d = a_0\sqrt{3}/2$, the distance between rows. Then

$$Q_x/\pi = -1, -1 + \frac{2}{D}, -1 + \frac{4}{D}, \ldots, 1 - \frac{2}{D}, \tag{21}$$

$$Q_y/\pi = -1, -1 + \frac{2}{L}, -1 + \frac{4}{L}, \ldots, 1 - \frac{2}{L}, \tag{22}$$

i.e., the Brillouin zone is appropriately discretized (there are L/a_0 discrete values Q_y, etc.), but the center of the Brillouin zone (the point $Q_x = Q_y = 0$) has to be omitted from the summation, since it would yield in Eq. (20) a uniform displacement of the whole lattice.

For a quantitative comparison of Eq. (20) to simulation results, it is preferable to evaluate Eqs. (19)–(22) numerically. This will be done in Sec. III. Here we rather discuss an approximate evaluation of Eq. (20) which elucidates the be-

havior of the displacement correlation qualitatively.

Considering the limit where both $1 \ll n \ll D$ and $1 \ll n \ll L$ we can approximate the summations by integrals, to obtain ($N=LD$)

$$\langle [u_y(n) - u_y(0)]^2 \rangle \approx 2 \int_{-\pi}^{\pi} \frac{dQ_x}{(2\pi)} \int_{-\pi}^{\pi} \frac{dQ_y}{2\pi} \frac{1-\cos(Q_y n)}{Q_x^2 + Q_y^2} \times \left(\frac{Q_y^2}{Q_x^2 + Q_y^2} \frac{k_B T}{\lambda + 2\mu - p} + \frac{Q_x^2}{Q_x^2 + Q_y^2} \frac{k_B T}{\mu - p} \right). \quad (23)$$

One can show that for the considered limit the integral has a logarithmic variation in n, similar to the simpler integral [40], where g is a constant,

$$I = \frac{2k_B T}{g} \int_{-\pi}^{\pi} \frac{dQ_x}{2\pi} \int_{-\pi}^{+\pi} \frac{dQ_y}{2\pi} \frac{1-\cos(Q_y n)}{Q_x^2 + Q_y^2} = \frac{k_B T}{g} \int_0^{\pi} \frac{dQ_x}{2\pi Q_x} [1 - \exp(-Q_x n)] \approx \frac{k_B T}{2\pi g} \ln n. \quad (24)$$

This logarithmic divergence of the correlation function of the displacements is responsible for the fact that in two-dimensional crystals the delta function singularities of $S(q)$ at the Bragg spots are replaced by power-law singularities, as is well known [36,41].

On the other hand, a different result is obtained if we consider a very elongated system, $D \ll n \ll L$. Then it is still appropriate to transform $(1/L)\Sigma_{Q_y}(\cdots)$ into $\int dQ_y/2\pi(\cdots)$ but keep the sum over Q_x discrete. This yields an expression of the type

$$\langle [u_y(n) - u_y(0)]^2 \rangle \approx \frac{2k_B T}{g} \frac{1}{D} \sum_{Q_x} \int_{-\pi}^{+\pi} \frac{dQ_y}{2\pi} \frac{1-\cos(Q_y n)}{Q_x^2 + Q_y^2}. \quad (25)$$

It is easy to see that the dominating term in Eq. (25) comes from a single term in the sum, namely the term with $Q_x=0$,

$$\langle [u_y(n) - u_y(0)]^2 \rangle \approx \frac{2k_B T}{g} \frac{1}{D} \int_{-\pi}^{+\pi} \frac{dQ_y}{2\pi} [1-\cos(Q_y n)]/Q_y^2. \quad (26)$$

Transforming the integration from Q_y to $z=Q_y n$ and using [40] $\int_{-\infty}^{+\infty} dz(1-\cos z)/z^2 = \pi$, a linear increase of the displacement correlation results,

$$\langle [u_y(n) - u_y(0)]^2 \rangle \approx \frac{2k_B T}{g} \pi \frac{n}{D}, \quad D \ll n \leq L. \quad (27)$$

Comparison of Eqs. (5) and (27) shows that in this limit a crossover to quasi-one-dimensional behavior has occurred, as expected. Equating Eqs. (24) and (27) the location of this crossover can be estimated as

$$n_{\text{cross}} \approx D \ln D. \quad (28)$$

Defining again the positional correlation length ξ from the condition that the mean-square displacement correlation reaches a finite fraction of the square of the lattice spacing, we find a result analogous to Eq. (9),

$$\xi \approx D(g/2\pi k_B T); \quad (29)$$

thus ξ diverges in both the limits $D \to \infty$ and $T \to 0$. Equation (29) is fully analogous to the corresponding result of the two-dimensional XY model, Eq. (3).

In the bulk case ($D \to \infty$) there still is no positional long range order, of course, since the logarithmic variation [Eq. (24)] of the mean-square displacement correlation has taken over. As is well known, this fact also implies that the peak heights of the structure factors $S(\vec{G}_0)$, $S(\vec{G}_1)$ are not proportional to N [cf. Eq. (12)], but scale with a sublinear power of N,

$$S(\vec{G}_0) \propto N^{1-const\ k_B T/g}. \quad (30)$$

The constant in the exponent in Eq. (30) can be worked out from the harmonic theory [27,36,41] but we shall not dwell further on this issue here. But we stress the consequence that both $\langle \Psi^2_{\vec{G}_0} \rangle$ and $\langle \Psi^2_{\vec{G}_1} \rangle$ are vanishing in the thermodynamic limit, while $\bar{\Psi}_6$ is nonzero at low temperatures [34].

When we consider a system with walls, the behavior near the wall will again depend very much on the nature of the boundary condition provided by the wall. Two types of walls shall be considered in this paper (Fig. 3), namely, (i) structureless flat planar walls and (ii) "structured walls" defined by two rows of particles fixed at the ideal lattice positions (with the proper lattice spacing having the same value as in the bulk). These fixed particles interact with the mobile particles with exactly the same interparticle potential as all the mobile particles do. With respect to positional order in the x direction normal to the walls, both types of boundary conditions at the walls act like an ordering field does in the case of magnetic systems (Fig. 1). Consequently, we expect that the density distribution $\rho(x)$ will be nonuniform near $x=x_{\text{wall}}=0$ also in the fluid phase, and show a periodic modulation with a period close to $d=a_0\sqrt{3}/2$ which decays over a distance of order $\xi(T)$, the positional correlation length. Also with respect to the orientational order Ψ_6, both types of walls clearly act like ordering fields, and so one expects that $\bar{\Psi}_6(x) \propto \exp[-x/\xi_6(T)]$ also in the fluid phase of a semi-infinite system. In a thin film confined between two parallel walls a finite distance apart, due to the combined effect of both walls some nonzero average order parameter $\bar{\Psi}_6(T)$ in the thin film hence will be present at all temperatures, also in the fluid phase. In the solid phase, of course, the situation will rather resemble Fig. 1(c), i.e., $\Psi_6(x) - \bar{\Psi}_6(T) \propto \exp[-x/\xi_6(T)]$, for x near the wall with $x_{\text{wall}}=0$.

However, the situation is quite different with respect to the positional order in the y direction parallel to the wall. The boundary condition provided by the structured wall also can be considered as a kind of field conjugate to the positional order, due to the commensurate corrugation of this potential in the y direction. So for x near x_{wall} also nonzero order parameters $\Psi_{\vec{G}_0}(x)$, $\Psi_{\vec{G}_1}(x)$ will be induced due to the response of the system to these local ordering fields, and this

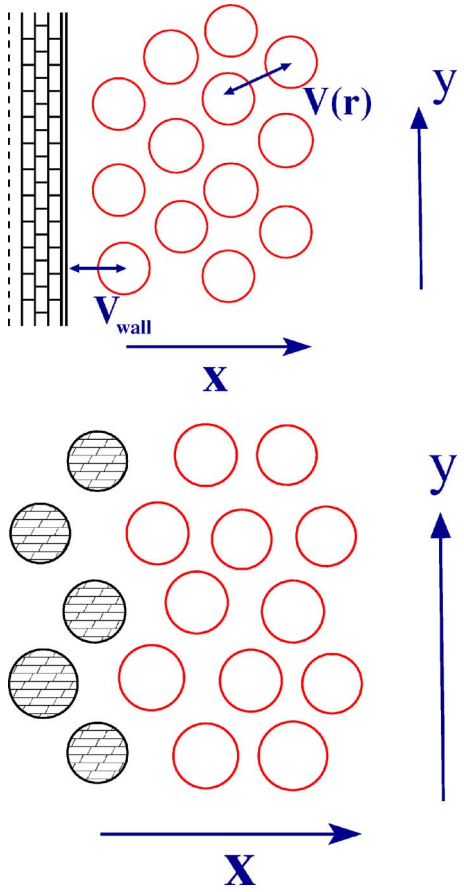

FIG. 3. (Color online) Schematic descriptions of the two types of walls used in this paper in order to confine the triangular crystal. Walls are always oriented along the y axis. The upper part shows the case of planar walls, described by a repulsive potential $V_{\rm wall}^{\rm planar} = \epsilon_{\rm wall}(\sigma/|x-x_{\rm wall}|)^{10}$. The position $x_{\rm wall}$ is chosen such that it replaces a row of particles otherwise present at this distance. The choice of the parameters $\epsilon_{\rm wall}$ and σ will be discussed in Sec. III. The lower part shows the case of "structured walls," created by fixing two rows of particles precisely at the positions of the ideal triangular lattice (with the same lattice spacing a_0 as in the bulk). The frozen particles interact with the mobile ones with the same pair potential $V(r)$ as is acting between two mobile particles a distance r apart. In this way, "structured" walls provide a potential corrugated in the y direction and precisely commensurate with the considered crystal structure.

crystalline local order will decay towards zero proportional to $\exp[-x/\xi(T)]$, in a semi-infinite system in its fluid phase. In its crystalline phase, however, true crystalline long range order with nonzero order parameters $\bar{\Psi}_{\vec{G}_0}$, $\bar{\Psi}_{\vec{G}_1}$ does not exist, as noted above, and we rather expect a power law decay of the surface-induced crystalline order, similar to the case of Fig. 1(b). The situation is rather analogous to the two-dimensional XY model for temperatures below the Kosterlitz-Thouless transition [25–29,42,43] in a local surface magnetic field H_1 [20–22]. In fact, at low temperatures the Hamiltonian of the XY model can be reduced to a harmonic form (J is the exchange constant) and (for $H_1=0$)

$$\mathcal{H}_{XY} = -J\sum_{\langle \ell,j\rangle} \cos(\Theta_\ell - \Theta_j) \approx \frac{1}{2}J\sum_{\langle \ell,j\rangle} (\Theta_\ell - \Theta_j)^2, \quad (31)$$

where an unimportant constant was omitted. The spin-spin correlation function in this spin-wave regime can then be written (cf. the analogy with the displacement correlation function)

$$\langle \vec{S}_0 \cdot \vec{S}_{\vec{r}}\rangle = \langle \cos(\Theta_0 - \Theta_{\vec{r}})\rangle = \exp\left(-\frac{1}{2}\langle(\Theta_0 - \Theta_{\vec{r}})^2\rangle\right). \quad (32)$$

Thus one finds in the bulk that [25–29]

$$\langle(\Theta_0 - \Theta_{\vec{r}})^2\rangle \approx \frac{k_B T}{\pi J}\ln(\pi r/a_0), \quad (33)$$

and hence the spin-spin correlation function exhibits the well-known power law decay

$$\langle \cos(\Theta_0 - \Theta_{\vec{r}})\rangle \propto \left(\frac{\pi r}{a_0}\right)^{-k_B T/(2\pi J)}. \quad (34)$$

Surface effects on the decay of correlations of a two-dimensional Gaussian model have been analyzed by Cardy [44]. In the framework of a continuum approximation, the harmonic Hamiltonian Eq. (31) becomes

$$\mathcal{H} = \frac{1}{2}J\int_{x>0} [\nabla\Theta(\vec{r})]^2 dxdy, \quad \vec{r} = (x,y), \quad (35)$$

where a free surface at $x=0$ is assumed for an otherwise semi-infinite system. Due to the free surface, translational invariance of the correlation function $\langle e^{i\Theta(\vec{r}_1)}e^{-i\Theta(\vec{r}_2)}\rangle$ of the order parameter $e^{i\Theta(\vec{r})}$ is broken, but due to the Gaussian character of the Hamiltonian, Eq. (35), we still have

$$\langle e^{i\Theta(\vec{r}_1)}e^{-i\Theta(\vec{r}_2)}\rangle = \exp\left(-\frac{1}{2}\langle[\Theta(\vec{r}_1) - \Theta(\vec{r}_2)]^2\rangle\right)$$
$$= \exp\left(G(\vec{r}_1,\vec{r}_2) - \frac{1}{2}G(\vec{r}_1,\vec{r}_1) - \frac{1}{2}G(\vec{r}_2,\vec{r}_2)\right),$$
$$G(\vec{r}_1,\vec{r}_2) = \langle\Theta(\vec{r}_1)\Theta(\vec{r}_2)\rangle. \quad (36)$$

In the continuum, a free surface with no surface fields can be described by a von Neumann boundary condition,

$$\left.\frac{\partial G(\vec{r}_1,\vec{r}_2)}{\partial x_1}\right|_{x_1=0} = 0, \quad (37)$$

and this condition can be automatically realized by writing

$$G(\vec{r}_1,\vec{r}_2) = G_\infty(\vec{r}_1 - \vec{r}_2) + G_\infty(\vec{r}_1 - \vec{r}_2'), \quad (38)$$

where $G_\infty(\vec{r}) = G(\vec{r}_1, \vec{r}_2 = \vec{r}_1 + \vec{r})$ for the fully translationally invariant infinite system, and $\vec{r}_2'$ is the mirror image of $\vec{r}_2$ with the surface (the line $x=0$) being the symmetry axis. Since $G_\infty(\vec{r})$ is (apart from constants) the correlation given in Eq. (33), one finds [44]

$$\langle e^{i\theta(\vec{r}_1)}e^{-i\theta(\vec{r}_2)}\rangle = \left(\frac{|\vec{r}_1 - \vec{r}_1'||\vec{r}_2 - \vec{r}_2'|}{|\vec{r}_1 - \vec{r}_2|^2|\vec{r}_1 - \vec{r}_2'|^2}\right)^{\eta/2},$$

$$\eta = \frac{k_B T}{2\pi J}. \tag{39}$$

If both sites $\vec{r}_1$, $\vec{r}_2$ are in the bulk, far away from the surface, we have $|\vec{r}_1| \to \infty$, $|\vec{r}_2| \to \infty$, and then $|\vec{r}_1 - \vec{r}_1'| \approx |\vec{r}_2 - \vec{r}_2'| \approx |\vec{r}_1 - \vec{r}_2'|$, for any large but finite $|\vec{r}_1 - \vec{r}_2|$. Then Eq. (39) reduces to Eq. (34), as it should be.

If site 1 is close to the surface, $\vec{r}_1 = (a_0, y)$, we have $|\vec{r}_1 - \vec{r}_1'| = 2a_0$, while $|\vec{r}_2 - \vec{r}_2'| = 2x$ if the site $\vec{r}_2 = (x, y)$ is deep in the bulk. Then

$$\langle e^{i\theta(\vec{r}_1)} e^{-i\theta(\vec{r}_2)} \rangle \approx \left(\frac{4a_0 x}{x^4} \right)^{\eta/2} \propto x^{-3\eta/2}, \quad \eta_\perp = \frac{3\eta}{2}. \tag{40}$$

The result $\eta_\perp = 3\eta/2 = 3k_B T/(4\pi J)$ does not seem to be discussed in the literature [22,44], while the case that both $\vec{r}_1$ and $\vec{r}_2$ are near the surface has been again analyzed. Then $\vec{r}_1 = (a_0, y_1)$ and $\vec{r}_2 = (a_0, y_1 + y)$, and Eq. (39) implies [44]

$$\langle e^{i\theta(\vec{r}_1)} e^{-i\theta(\vec{r}_2)} \rangle \approx \left(\frac{4a_0^2}{y^4} \right)^{\eta/2} \propto y^{-2\eta}, \quad \eta_\parallel = 2\eta. \tag{41}$$

Since the low temperature phase of the XY model can be interpreted as a line of critical points, we expect a scaling relation [13,14] to hold,

$$\eta_\parallel = 2\eta_\perp - \eta, \tag{42}$$

and this relation is indeed satisfied by Eqs. (40) and (41). Based on numerical data, Berche [22] concluded that the relation $\eta_\parallel = 2\eta$ holds also outside of the spin wave regime, at all temperatures up to the Kosterlitz-Thouless (KT) transition temperature, where $\eta = 1/4$ [43] and hence $\eta_\parallel = 1/2$. Equation (40) then implies $\eta_\perp = 3/8$ at the KT transition.

If now a surface magnetic field is applied, a response of a spin at a site $\vec{r}$ deep in the bulk is created. This response decays towards zero according to [13,14]

$$\langle |\vec{S}(\vec{r})| \rangle = \langle |\exp[i\theta(\vec{r})]| \rangle \propto x^{-\eta/2}, \quad \text{for } d = 2, \tag{43}$$

i.e., the same exponent η that controls also the decay of correlations in the bulk controls also the order parameter profile. The correlation function between spins which are both at the surface exhibit then a finite range, however. From the scaling approach to surface critical phenomena [13,14] one can predict

$$\langle \vec{S}_0 \cdot \vec{S}_{\vec{r}} \rangle - \langle \vec{S}_0 \rangle \cdot \langle \vec{S}_r \rangle \propto \exp(-y/\xi_\parallel),$$

$$\xi_\parallel \propto H_1^{-(1+\eta/2-\eta_\perp)} = H_1^{-(1-\eta)}, \tag{44}$$

where in the last step Eq. (40) was used. At the KT transition, the exponent describing the divergence of $\xi_\perp$ as $H_1 \to 0$ becomes $1 - \eta = 3/4$.

Redirecting attention to the harmonic solid, we emphasize that the case of the planar wall does not involve any "surface field," as far as positional order in the y direction parallel to the wall is concerned. Since the comparison between Eqs. (24) and (33) shows that the quantity $k_B T/(2\pi g)$ plays the same role as the exponent η in the XY model, we conclude that the positional correlations between displacements between two particles in the surface increase as

$$\langle [u_y(n) - u_y(0)]^2 \rangle \propto \eta_\parallel \ln n, \tag{45}$$

while the mean-square correlation between a particle near the wall and another particle deep in the bulk should behave as

$$\langle [u_y(n) - u_y(0)]^2 \rangle \propto \eta_\perp \ln n. \tag{46}$$

We suggest that the scaling relation, Eq. (42), between the exponents η, $\eta_\parallel$, and $\eta_\perp$ can be carried over to the present case as well.

Finally we mention that according to the Kosterlitz-Thouless-Halperin-Nelson-Young (KTHNY) theory of melting [25,27,35–39] one should also consider in addition to the fluid phase (where both orientational and positional correlations have finite correlation range) and to the crystalline phase (where positional correlations exhibit power law decay, while there exists orientational long range order) at intermediate temperatures (and/or densities, respectively) the hexatic phase. This phase exhibits still short range positional correlations only, while orientational correlations should have a power law decay. However, despite a lot of effort, the evidence (from numerical simulations [45–68] and experiments) for the existence of the hexatic phase is scarce, some studies did interpret their findings in terms of a weak first order liquid-solid transition. Although it would be very interesting to study how wall effects show up in the KTHNY scenario of melting, this problem shall not be addressed here, since it still would require a prohibitively large computational effort.

III. MODEL AND SIMULATION TECHNIQUE

We consider a system of soft disks, i.e., point particles interacting with the inverse power law potential

$$U(r) = \begin{cases} \epsilon(\sigma/r)^p & : \quad r \leqslant r_c \\ 0 & : \quad \text{otherwise}, \end{cases} \tag{47}$$

choosing a cutoff distance $r_c = 2.5\sigma$ for computational convenience, and $p = 12$ (as in the repulsive part of a Lennard-Jones potential).

As is well known, one can prepare systems of spherical colloidal particles with various types of interactions: neutral particles coated with polymer brushes that have a short range entropic repulsion due to the excluded volume interaction between the polymers provide a model to approximate hard spheres [1–4]. Charged colloids (with counterions in the solution) interact with the Derjaguin-Landau-Vervey-Overbeek potential [69,70], a screened (Yukawa-type) Coulomb interaction. However, of particular interest in our context are particles containing a superparamagnetic core: if such particles are held at the air-water interface of a water film underneath a glass plate and one applies a magnetic field oriented perpendicular to the glass plate, one creates a two-dimensional system of colloidal particles interacting with a uniformly repulsive r^{-3} interaction [71–74]. These systems have proven to be valuable model systems for an experimental study of two-dimensional melting. Thus it would be desirable to consider the case $p = 3$ in Eq. (47) also, which would allow a rather direct comparison to corresponding experiments. However, the long range of this potential (which then should

not be cut off at any short distance, of course) is very inconvenient for simulations; one would need very large computer time resources for a meaningful study. As a compromise, we hence took $p=12$: then the chosen cutoff produces only rather negligible errors, and a reasonably fast Monte Carlo simulation code can be written. A further advantage is that the melting behavior of the model Eq. (47) in the bulk has been extensively studied in careful previous work [64]. Choosing now units of temperature such that $\epsilon=1$ ($k_B=1$) and length such that $\sigma=1$, at a density $\rho=1.05$ chosen throughout in the present work melting occurs at $T_m=1.35\pm0.01$ [64]. Note that the homogeneity of the potential, Eq. (47), implies that (in $d=2$ dimensions) excess thermodynamic properties (relative to the ideal gas contribution) and the scaled pair distribution functions $g(r/\sigma)$ depend on a single parameter

$$x = \rho\sigma^2(\epsilon/k_BT)^{2/p} \tag{48}$$

rather than on ρ and T separately [75].

Next we discuss how to represent the confining walls. One choice is to take a smooth repulsive wall located at $x=x_{\mathrm{wall}}$, described by a wall potential [76]

$$U_{\mathrm{wall}} = \epsilon_{\mathrm{wall}}(\sigma/|x - x_{\mathrm{wall}}|)^{10}. \tag{49}$$

The motivation for a decay with the 10th power is the idea that such a potential would result if we have a semi-infinite crystal with a power law interaction given by Eq. (47), but no cutoff, and the total potential is summed over the half space: in the continuum approximation, a potential of the type of Eq. (49) results.

Figure 3(a) illustrates the choice of the geometry: the wall is oriented along the y axis (at $x_{\mathrm{wall}}=0$) the first row of atoms is placed at $x=a_0\sqrt{3}/2$, the lattice spacing a_0 being chosen such that the crystal density is $\rho=1.05$, which yields (the chosen area is $A=Na_0^2\sqrt{3}/2$ for a fixed number of N particles, $\rho=N/A$) $a_0=(2/\sqrt{3}\rho)^{1/2}\approx1.049$. Normally we choose the distance D between the walls such that it corresponds to an integer number of rows in the ideal lattice, $D=N_xa_0\sqrt{3}/2$, but also the case of a systematic misfit, $D=(N_x+\Delta)a_0\sqrt{3}/2$, $-2<\Delta<0$, will be briefly addressed (Sec. V).

The other choice of wall, hereafter referred as "structured wall" is created by simply taking at $x=0$ a row of particles rigidly fixed at the positions of the perfectly ideal lattice with lattice spacing a_0, and a second such row at $x=-a_0\sqrt{3}/2$, as shown in Fig. 3(b). These rigidly fixed particles at $x\leqslant0$ interact with the mobile particles (at positions $0<x<D$) with exactly the same potential, Eq. (47), as chosen between the mobile particles. At $x=D$ and $x=D+a_0\sqrt{3}/2$, two further such rows of fixed particles are placed, perfectly commensurate with the rows on the other side of the thin strip. Note that at rather low temperatures, as are studied here, the probability that particles could move to positions $x<0$ or $x>D$ is negligibly small. Therefore [note the cutoff in the potential, Eq. (47)] it would not have any physical effect on the system if we placed further rows of fixed particles at positions $x=-\nu a_0\sqrt{3}/2$ or $x=D+\nu a_0\sqrt{3}/2$ with $\nu=2$, 3 etc.

This choice of boundary condition thus creates a corrugated confinement potential $V_{\mathrm{struc}}(x,y)$ which stabilizes the crystalline order. Clearly, this potential plays the role of a "surface field" on both the positional and orientational order parameters of the crystal. The situation is similar to the case of crystalline monolayers adsorbed on crystalline substrate surfaces, if the monolayer crystal structure is commensurate with the crystal structure of the surface [19].

While $V_{\mathrm{struc}}(x,y)$ does not contain any more any parameter that could be varied, Eq. (49) still contains as a parameter the strength ϵ_{wall} of the flat wall potential, which needs to be chosen with care. If ϵ_{wall} is chosen too large, the rows of particles next to the wall are "pushed away" from the wall, and then the distance between the first and second row in the x direction (as well as the distance between the second and third row, etc.) will be smaller than the value $a_0\sqrt{3}/2$ which is expected for a perfect triangular lattice with lattice spacing a_0. Note that the lattice spacing a_0 is fixed *a priori* by choosing a periodic boundary condition in the y direction, the linear dimension being precisely $L=N_ya_0$, and then for the ideal triangular lattice with N_x rows in the x direction we have $N=N_xN_y$ for the total number of particles, and $D=N_xa_0\sqrt{3}/2$, as noted above. While this structure results for the "structured wall" boundary condition trivially by construction, for the planar wall the actual distance d between rows does depend on the parameter ϵ_{wall}, as Fig. 4 shows [76]. It is seen that for $\epsilon_{\mathrm{wall}}=0.0005$ the distance d between rows coincides within error with the ideal value $a_0\sqrt{3}/2$, while for larger ϵ_{wall} the distance d is systematically smaller (remember that the distance between both walls is fixed, and when the distance of the first and last row from the adjacent wall increases less space is available for the remaining rows and hence d must decrease).

Conversely, for the "hard wall" boundary condition the distortion goes into the opposite direction, the first (and last) rows are closer to the hard walls than would be expected if there were a row of particles, and hence more space is available for the remaining rows, d must increase. The comparison of the two choices for N_x shows (Fig. 4) that this distortion is distributed rather uniformly over the strip, and hence this deformation of the lattice (strictly speaking, we get the symmetry of a centered rectangular lattice rather than an ideal triangular lattice) systematically depends on D. A further consequence of this distortion is the fact that the angle α between rows (Fig. 5) which is $\alpha=60$ for an ideal triangular lattice deviates from this ideal value, of course. However, Fig. 5 confirms the expectation from Fig. 4 that for $\epsilon_{\mathrm{wall}}=0.0005$ no such distortion occurs. Therefore we have chosen $\epsilon_{\mathrm{wall}}=0.0005$ for the further studies throughout.

Apart from the study of the lattice structure and the mean-square displacements and positional and orientational order parameters and their correlations there is also considerable interest in the elastic constants of two-dimensional crystals. Remember that the dependence of these elastic constants on temperature (or density, respectively) plays a crucial role in the theory of two-dimensional melting [27,35–39,68]. Again one expects a significant effect of the symmetry of the crystal structure: while for a centered rectangular lattice all four elastic constants C_{11}, C_{22}, C_{12}, C_{23} (we employ the Voigt notation here [33]) will differ from each other, for a perfect triangular crystal we expect in the bulk the symmetry relations

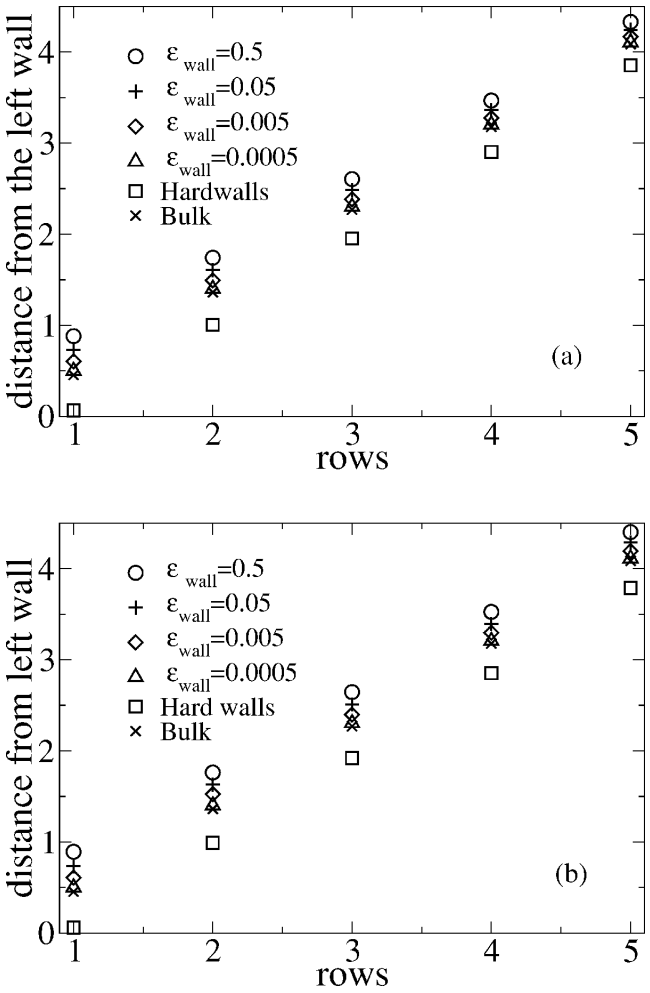

FIG. 4. Distance (in units of σ, $\sigma=1$) of rows number $\ell=1$, 2, 3, 4, 5 from the left wall for two choices of D corresponding to (a) $N_x=20$ ($D=18.163$) and (b) $N_x=30$ ($D=27.245$), for four different choices of ϵ_{wall}. Also the alternative "hard wall" boundary condition and the theoretical values $\ell a_0\sqrt{3}/2$ (denoted as "bulk") are included. All these data are taken at a temperature $T=1$. ϵ_{wall} and T are given in units of ϵ ($\epsilon=1$).

$$C_{11} = C_{22}, \quad C_{12} = C_{23}. \tag{50}$$

Note that the second of these relations follows from the Cauchy relations for centrally symmetric pair interactions [33].

In the present work, elastic constants were extracted from the simulations applying the method where strain fluctuations in subsystems are analyzed [67,76,77]. Table I compares the results obtained from this method for two choices of ϵ_{wall} with the corresponding bulk values. To test the method for systems in the presence of walls also the standard method using the correlation functions of stress fluctuations [78] is used as well. For the bulk case the stress tensor is simply calculated from the virial expression [75,78] computing the statistical average $\langle\sigma_{ij}\rangle$,

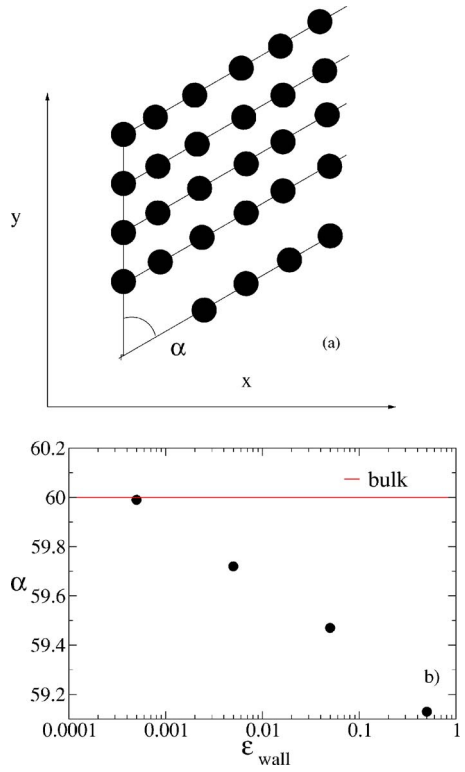

FIG. 5. (Color online) Definition of the angle α between lattice rows (a) and a plot of the observed angle α for $D=27.245$ and $T=1$ vs ϵ_{wall} (b). ϵ_{wall} and T are given in units of ϵ ($\epsilon=1$).

$$\sigma_{ij} = \frac{1}{LD}\left[\sum_{\alpha\neq\beta} U'(R^{\alpha\beta})\frac{R_i^{\alpha\beta}R_j^{\alpha\beta}}{R^{\alpha\beta}} - N_xN_yk_BT\delta_{ij}\right], \tag{51}$$

where the summation extends over all pairs of particles α, β, $R_i^{\alpha\beta}$ is the ith component ($i=x,y$) of the vector $\vec{R}^{\alpha\beta}=\vec{R}^{\alpha}-\vec{R}^{\beta}$, $\vec{R}^{\alpha}$, $\vec{R}^{\beta}$ being the positions of particles α and β, and $R^{\alpha\beta}=|\vec{R}^{\alpha}-\vec{R}^{\beta}|$, $U'(R)=dU/dR$. In the case of systems confined between walls, additional terms due to the walls occur, that have been discussed extensively by Varnik *et al.* [79]. The elastic constants then can be expressed in terms of a reduced correlation function of the observable Eq. (51) whose average yields the stress tensor, involving also a term containing the second derivative of the potential $U''(R^{\alpha\beta})$ [78]. The generalization to the case including planar walls

TABLE I. Elastic constants of a two-dimensional strip and the corresponding bulk elastic constants (in Voigt notation). All data were extracted from a system with $N_x=20$ and $N_y=120$. The first entry is the subsystem method, the second is the stress fluctuation method. Relative errors of the results are about 1–2 %.

ϵ_{wall}	0.0005		0.0050		bulk
C_{11}	120.1	123.3	136.1	132.2	126.5
C_{22}	130.0	127.6	125.0	122.6	127.0
C_{12}	35.6	38.3	43.6	40.6	42.8
C_{33}	25.6	20.3	24.2	18.8	42.3

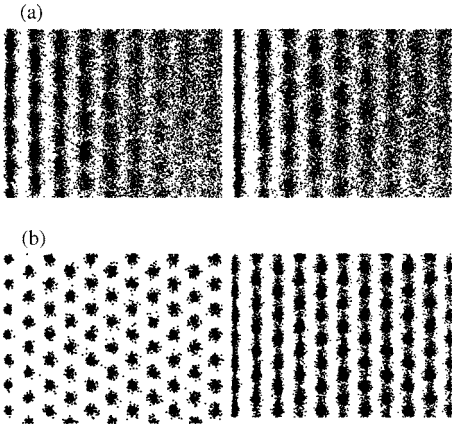

FIG. 6. (a) Configurations of the particles in the first nine rows adjacent to the left wall at $T=1.6$, for the structured wall (left) and the planar wall (right). 1000 configurations of a run lasting 10^6 Monte Carlo steps (MCSs) per particle are superimposed, fixing the center of mass of the mobile particles in each configuration in the same position. The linear dimensions were $L=30$ and $n_x=30$, with periodic boundary conditions in the y direction. (b) Same as (a) but for $T=1.0$. T is given in units of ϵ ($\epsilon=1$).

(following [79] the walls can be treated like particles having infinite mass and contributions to the forces only in the x direction) is straightforward but the resulting expression [80] is rather clumsy and hence is not reproduced here. Similarly, we do not describe further the method for how one extracts the elastic constants from strain fluctuations in subsystems, since detailed expositions can be found in the literature [67,76,77]. Note that for the data in Table I the Monte Carlo moves have been constrained (as described in [77]) to disallow the formation of dislocations, but in practice this constraint had almost no effect at the low temperature considered ($T=1$).

One sees from Table I that in the bulk the symmetry relations Eqs. (50) are fulfilled within statistical errors. For the confined system, a mild violation of the relation $C_{11}=C_{22}$ is found, while the second relation $C_{12}=C_{33}$ is strongly violated. Within our statistical errors, both methods to compute elastic constants agree with each other. Choosing $\epsilon_{wall}=0.0005$ where the structure is closest to the ideal triangular lattice does not bring the elastic constants C_{12} and C_{33} close to their bulk values, however. We shall return to this problem in the next section.

IV. NUMERICAL RESULTS

A good qualitative insight into the effect of confining walls on the order of two-dimensional solids is obtained by superimposing snapshot pictures of the instantaneous positions of the particles (Fig. 6). In the disordered fluid phase far above melting [Fig. 6(a)] the system in the bulk then yields a uniform grey pattern, reflecting the fact that in a fluid the density is homogeneous. However, near the walls we recognize in both cases a nonuniform density distribution; the density is enhanced in layers parallel to the walls and depleted in between. This density modulation ("layering") decreases as one moves away from the walls towards the bulk. While for the planar wall boundary conditions the density distribution is inhomogeneous in the x direction normal to the walls but homogeneous in the y direction, in the fluid phase, we also recognize a local ordering in the y direction close to the wall for the structured wall boundary condition. In the crystalline phase [$T=1.0$, Fig. 6(b)], however, the crystalline order now is stable in the bulk as well as near the walls. Of course, on the small length scales visualized here the fact that the increase of the displacement correlation function $\langle[\vec{u}(\vec{r})-\vec{u}(0)]^2\rangle$ with distance $\vec{r}$ ultimately destroys positional long range order is not visible. We recognize, on the other hand, already from the snapshot pictures that the walls affect this order in a rather different manner: while the mean-square displacement of the particles away from the lattice positions of the ideal crystal structure is uniformly smaller for the particles close to a structured wall, there occurs a pronounced anisotropy of fluctuations close to a planar wall: There is a clear reduction in the spread of the dark region in the x direction for the first few rows adjacent to the wall, while in the y direction the extent of the dark region (which is a measure of the local mean-square displacement in that direction) is strongly enhanced.

We have studied the layering phenomena in the strips by recording the average density profiles in the x direction (Figs. 7 and 8). Since $\rho(x)$ exhibits the symmetry $\rho(x)=\rho(D-x)$, only the left half of the strip is shown. For low temperatures, such as $T=1$, we see that the layering effect [enhancement of $\rho(x)$ around the ideal positions of the lattice rows] is visible over a few layers only (five layers in the case of $T=1$), and then the bulk behavior is reached. Approaching the melting transition from the opposite side, however, we see a somewhat larger range over which layering can be observed. While for $T=1.8$ (and higher) for $10\leqslant x\leqslant 20$ the density is uniform in the thin strips and agrees with the density in the bulk, irrespective of the boundary conditions at the wall, already for $T=1.6$ a weak density modulation is still left even in the center of the strip. Thus the increasing range of the layering effect as one approaches the melting temperature T_m from above reflects the existence of an increasing correlation length ξ of positional order. As is well known, ξ remains finite at T_m if the transition is first order, while ξ should diverge to infinity at the transition from the hexatic phase to the crystal, if the KTHNY scenario of two-dimensional melting applies [25–27,35–39]. In principle, one could try to use the layering phenomenon due to walls to extract information on ξ. In practice, this is rather difficult in the transition region, however, since the finite strip width D causes important finite size effects. This is demonstrated in Fig. 8, where data for $T=1.4$ are shown: Using data only for $n_x=30$ well-defined ordering in a layered structure is enforced over the entire strip, while the bulk at $T=1.4$ clearly has melted, and the bulk density distribution already is uniform. A comparison with corresponding data for $n_x=60$ (Fig. 8) shows, however, that now the strip is disordered in its center, and also the amount of layering near the walls is systematically smaller than was found for $n_x=30$. As a consequence, a reliable estimation of ξ for T near T_m would require a systematic variation of the strip width

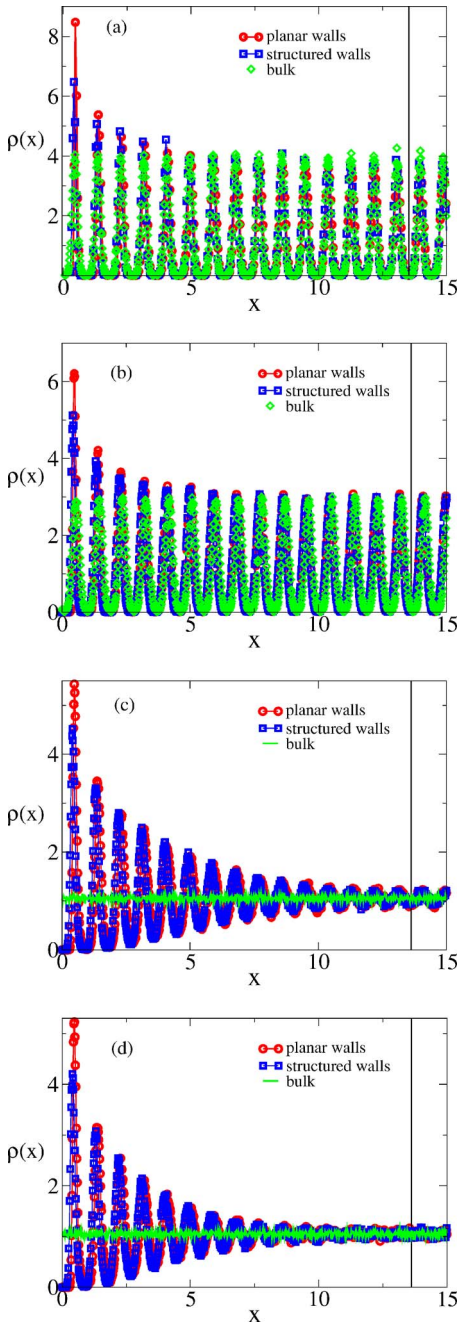

FIG. 7. (Color online) Density distribution $\rho(x)$ plotted vs x for $n_x=30$ and various temperatures: $T=1.0$ (a), 1.2 (b), 1.6 (c), and 1.8 (d). The center of the strip ($x=D/2$) is marked by a vertical line.

$D=n_x a\sqrt{3}/2$ over a wide range, in order to be able to extrapolate the results towards $D\to\infty$. The huge computer resources required to do this have prevented us from carrying out such a systematic study of two-dimensional melting via surface effects. A naive fit of the density differences $\rho(x_{\max})-\rho$ at the maxima positions $x_{\max}$ in the range $3\leqslant x\leqslant 57$ to a function proportional to $\{\exp(-x/\xi)+\exp[(D-x)/\xi]\}$ yields the data shown in Fig. 9. In principle, we expect that ξ should not depend on the type of boundary condition at the wall: only the prefactor of the above function should. This expectation is borne out for $T=2$ and

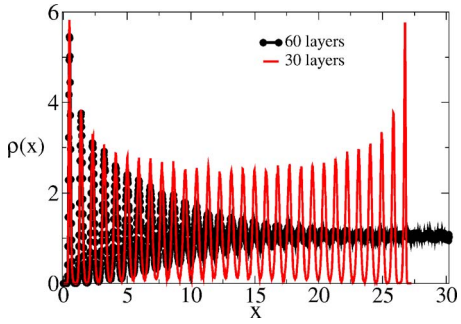

FIG. 8. (Color online) Density distribution $\rho(x)$ vs x for $T=1.4$ and planar walls in the case of $n_x=30$ (thin line) and $n_x=60$ (thick line), respectively.

$T=1.8$, within the statistical errors. while for $T\leqslant 1.6$ the results for the case of structured walls are slightly but systematically larger. Presumably this effect is due to a nonlinear response of the density distribution $\rho(x)$ to the perturbing "field" created by the walls, which is expected for x close to both walls.

In principle, this problem can be avoided by restricting the fit to the inner region of the strip, where the density oscillations around the average density are small enough (Figs. 7 and 8) so that such nonlinear effects are negligible, but then the problem is that due to the statistical noise of the data the statistical errors of ξ become much larger.

We now turn to the behavior of the local orientational order parameter $\langle|\Psi_6(x)|^2\rangle$, Fig. 10. As expected on theoretical grounds (see the discussion of Fig. 2), we see that both boundary conditions enhance the orientational order near the walls in a similar manner. While for $T<T_m$ a clearly developed flat plateau is observed for $10\leqslant x\leqslant 20$, for $T>T_m$ the residual order parameter near the center of the film is not constant over an extended region of x. Thus the fact that $\langle|\Psi_6(x)|^2\rangle$ is still nonzero everywhere in the thin strip even at temperatures far above T_m again is clearly a finite size effect! Consequently, plotting $\langle|\Psi_6(x=D/2)|^2\rangle$ vs T [Fig. 11(a)] the melting transition does not show up by a clear vanishing of this mean-square order parameter, but near $T=T_m$ there is a mild inflection point in the curves, and for $T>T_m$ one finds

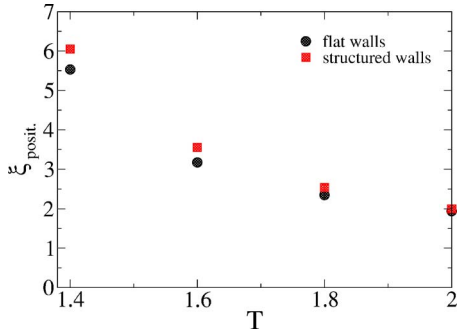

FIG. 9. (Color online) Correlation length ξ for the decay of the positional order near the walls plotted vs temperature, for a system with $n_x=60$, $n_y=60$, and for the two types of boundary conditions at the walls. ξ is given in units of σ ($\sigma=1$), T in units of ϵ ($\epsilon=1$).

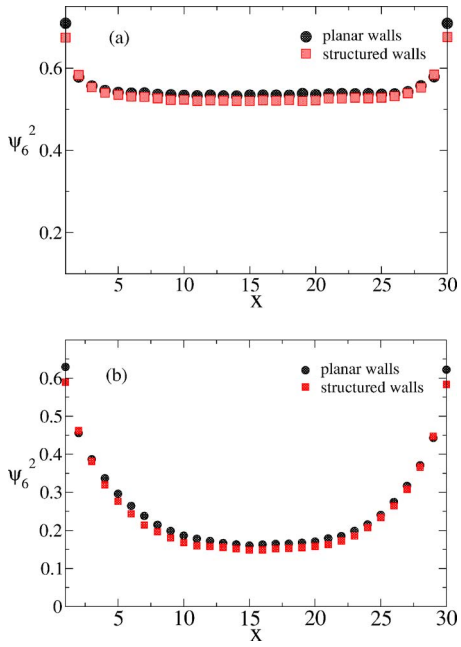

FIG. 10. (Color online) Plot of the local orientational order parameter square $\langle|\Psi_6(x)|^2\rangle$ vs x, for $n_x=n_y=30$ and two temperatures, $T=1.2$ (a) and 1.6 (b). Circles refer to the planar wall and squares to the structured wall boundary condition, respectively.

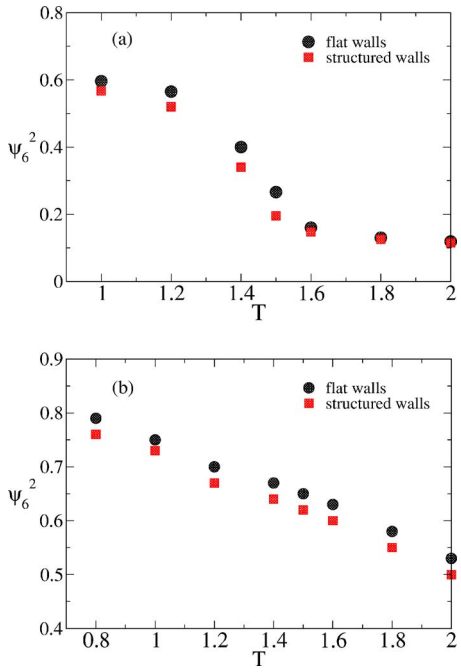

FIG. 11. (Color online) Mean-square order parameter in the center of the strip (a) and near the walls (b) plotted vs temperature. Circles refer to the planar wall and squares to the structured wall boundary condition, respectively. All data refer to $n_x=n_y=30$. T is given in units of ϵ ($\epsilon=1$).

the "finite size tails" well known from simulation studies of other phase transitions, too [81,82].

Again one can associate a correlation length ξ (which should be twice the correlation length ξ_6 defined in Sec. II, since we deal with the order parameter square), fitting the data again to a function of the type $A\{\exp(-x/\xi)+\exp[(D-x)/\xi]\}$, where A is an amplitude factor depending on the type of boundary condition. Figure 12 shows that this correlation length also is very small at high temperatures, and increases slightly faster than the positional correlation length does (Fig. 9).

Of course, it is also possible to study the orientational correlation function $g_6(\vec{r})$ [Eq. (14)]. However, while this correlation function is translationally invariant in the bulk, in a system with walls such a translational invariance holds in the y direction only. Hence we study the decay of the correlation in the y direction for two sites within the strip which are the same distance x away from the left wall,

$$g(x,y)=\langle\Psi_6(x,0)\Psi_6(x,y)\rangle. \tag{52}$$

Figure 13 gives a global view of this function for three temperatures. One can clearly see that near the walls there is very little y dependence at all temperatures, due to the high degree of orientational order enforced at the walls. In the center of the strip, there is again little variation at low temperatures ($T=1$), where the system everywhere is well or-

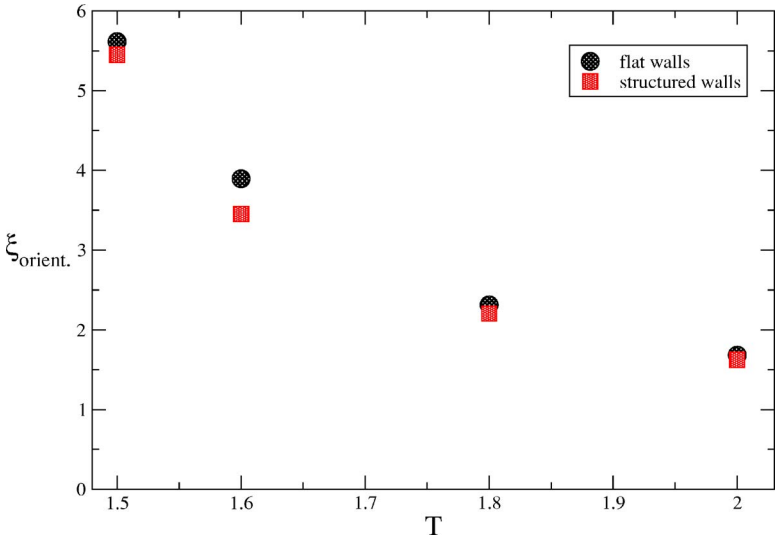

FIG. 12. (Color online) Correlation length extracted from the decay of the local orientational order parameter square with distance (Fig. 10) plotted vs temperature. Circles refer to the planar wall and squares to the structured wall boundary condition, respectively. All data refer to $n_x=n_y=30$. ξ is given in units of σ ($\sigma=1$), T in units of ϵ ($\epsilon=1$).

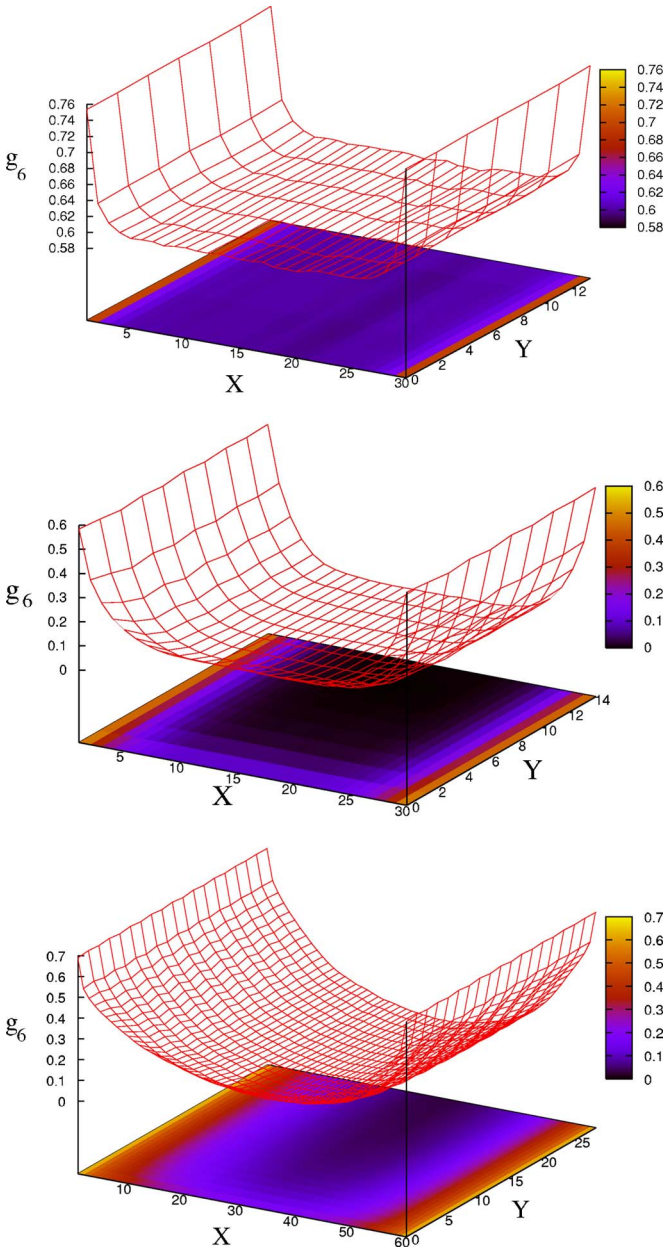

FIG. 13. (Color online) Correlation function $g(x,y)$ for $n_x=n_y=30$ and $T=1$ (upper part) or 1.8 (middle part), respectively. In the projection the numerical values of this function according to a grey scale are indicated. The lower part shows analogous results for $T=1.4$ and $n_x=n_y=60$. Note that the y coordinate is shown only in the range $0 \leqslant y \leqslant n_y/2$, since $g(x,y)=g(x,n_y-y)$, due to the periodic boundary condition in the y direction.

dered, and at high temperatures ($T=1.8$), where the system in the center is almost disordered. In contrast, close to the transition (e.g., for $T=1.4$) a slow variation of $g(x,y)$ with both x and y is observed. Due to the residual order which occurs in $g(x,y)$ for large distances, apart from the limiting case of very large D and correspondingly large enough x in the middle of the strip, we have not succeeded in a convincing quantitatively reliable analysis of the functional variation of $g(x,y)$. This problem hence must be left to future work.

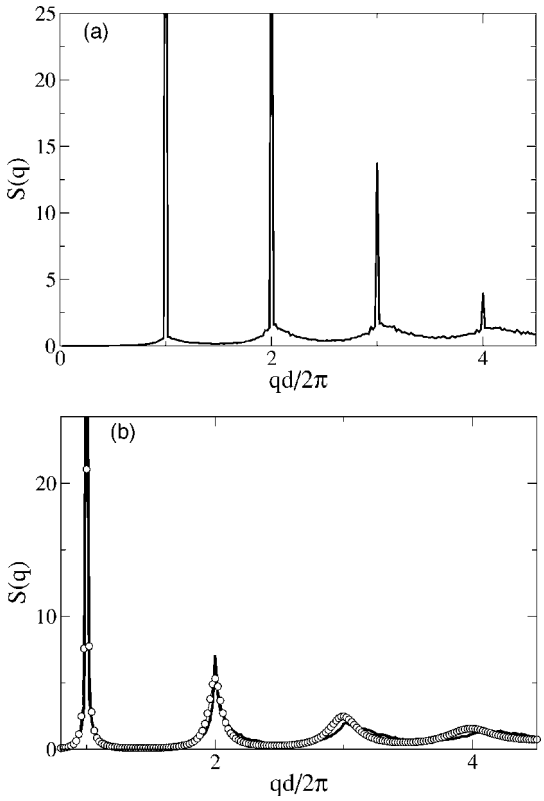

FIG. 14. Static structure factor $S(q)$ at $T=1$ plotted vs $qd/2\pi$ for structured walls (a) and planar walls (b). All data are for systems of $n_x=30$, $n_y=100$. For the planar walls the full curve is a fit to Eq. (8), δ is taken from Ref. [83].

A quantity of considerable experimental interest is the structure factor $S(\vec{q})$, of course [Eq. (11)]. We have analyzed this quantity as well, orienting $\vec{q}$ along the y direction. As an example, $S(q)$ is plotted vs q at $T=1$ in Fig. 14, for both types of boundary conditions [83].

Figure 14 shows that for the structured wall sharp Bragg peaks result. As expected, the height of these peaks decreases with increasing q due to the effect of the Debye-Waller factor, but the width does *not* increase with increasing q, and this behavior is exactly as it should be for Bragg scattering from ordinary ideal crystals at finite temperature. We have also checked that the peak heights scale proportional to the number of particles per row (the first peak has a height of 79 for 100 particles per row but only 24 for 30 particles). In contrast, no such simple size dependence occurs for the structureless repulsive boundary. In this case a typical fluid-like structure factor results, but with heights of the first two peaks which are much larger than for typical fluids (remember that in three-dimensional fluids at the melting temperature the first peak of $S(q)$ reaches a height of about 3 [75]). In fact, this structure factor is almost in quantitative agreement with a fit of $S(q)$ to the result for the one-dimensional harmonic chain, Eq. (8), adjusting a single parameter in that equation, namely $\delta=0.07$. Remember, however, that in Fig. 14 we do not deal with a true one-dimensional system, but rather with a system of 30 rows confined between two boundaries, and that the state of the system is *not like a fluid*, as a glance on the configuration picture [Fig. 6(b)] shows. In

a fluid, one would see lots of dislocations in a snapshot of a single configuration at various places, and superimposing a large number of such snapshots a uniform density distribution results [as displayed in Fig. 6(a), away from the walls], which is not the case here, where locally a crystalline structure is found, and only the long range order in the y direction (but not in the x direction perpendicular to the walls) is destroyed. Thus the system may be viewed as a kind of two-dimensional smectic phase, a phase with orientational long range order but positional long range order in one direction only. Thus it would be completely wrong to interpret the destabilization of crystalline two-dimensional long range order by flat structureless walls as surface-induced melting. If surface-induced melting occurred, we would find lots of dislocations near the boundaries, which is not at all the case here (while this may occur for very small D incommensurate with the layer spacing $d=a\sqrt{3}/2$, see [6]). In fact, we have used the algorithm of [67] to check the formation of dislocation pairs from a local coordination. Apart from the rows adjacent to the walls, the coordination number of each particle in a triangular structure is 6, while dislocations show up via a fivefold or sevenfold coordination, and at the walls the coordination number of each particle in a triangular structure is 4, dislocations showing up via threefold or fivefold coordination. We have found that at $T=1$ the average density of dislocations is 10^{-5}, and this explains why no dislocation pair is seen in typical snapshot pictures such as Fig. 6(a).

The fact that the two-dimensional crystal bounded by planar walls has a crystalline order only on large but finite length scales, as is evidenced by its fluidlike structure factor (Fig. 14), has also drastic consequences on its elastic behavior. Figure 15 compares the elastic constants of this system with the corresponding case of crystalline strips of various thicknesses but with the structured wall boundary condition. Since this latter boundary condition pins the long-range order at boundaries, the order is stabilized throughout the system. For a number of rows n exceeding about $n=30$ one finds that all elastic constants have then converged towards the elastic constants of a bulk system (with periodic boundary conditions in all directions). Conversely, this is not true for the system with planar walls: while C_{11}, C_{22}, and C_{13} converge to bulk behavior in a similarly rapid way, C_{33} does not. Rather we find

$$C_{33}(n) \approx C_{33}^{\text{bulk}}/2, \tag{53}$$

apparently independent of the number n of rows in the thin strip! If we look at the elastic moduli we have to take into account also a correction due to the pressure, namely for the shear modulus we have

$$\mu = C_{33} - \bar{P}, \tag{54}$$

where

$$\bar{P} = \frac{1}{2}(\sigma_{xx} + \sigma_{yy}), \tag{55}$$

with $\sigma_{\alpha\beta}$ we indicate here the stress tensor. This indicates that the system has a vanishing shear modulus, i.e., the crystal is intrinsically unstable. The question of how for the elastic constants the thermodynamic limit is approached is intriguing. The planar boundaries provides an elastic distortion of long range [84] to the crystal, and hence the crystalline behavior is significantly modified.

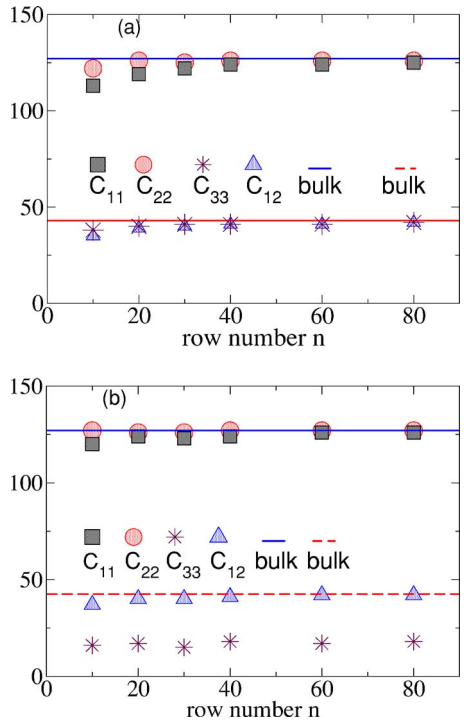

FIG. 15. (Color online) Elastic constants (in units of k_BT/σ^2) for structured walls (a) and planar walls (b) plotted vs the number of rows n between the walls. The Voigt notation for the elastic constants is used. Horizontal straight lines show the bulk values of the corresponding triangular crystal, for which the symmetries $C_{11}=C_{22}$ and $C_{12}=C_{33}$ hold.

In order to provide further clarification to this lack of stability of crystalline order in finite systems with planar walls we have evaluated the displacement correlation function $\langle[u_y(n)-u_y(0)]^2\rangle$, using both the theory of Sec. II [Eqs. (19) and (20)], with the above elastic constants of the bulk crystal as an input, and directly from the simulation (Figs. 16–18). Figure 16 shows that for large enough L the linear relation obtained in Eq. (27) is in fact reproduced, for large enough L and $D \ll n \ll L$. However, when n becomes of the order $n \approx 2D$ or smaller, deviations set in [due to the crossover towards the logarithmic behavior, Eq. (24)], while for $n \approx L/4$ deviations set in due to the symmetry implied by the periodic boundary condition that limits the linear increase implied by Eq. (27). In order to test for the initial logarithmic increase of $B(y)=\langle[u_y(y)-u_y(0)]^2\rangle$ with y, the data for $D=20$, $L=500$ of Fig. 16 are replotted on linear-log scales in Fig. 17, and data from a direct Monte Carlo simulation of this system are included. One can see that the harmonic theory and the Monte Carlo results are in quantitative agreement, with no adjustable parameters whatsoever! A similar agreement has also been found in studies of the low temperature phase of the XY model [21,22], which has been discussed as a simpler reference system in Secs. I and II. From this work [21,22] it is also clear that this agreement breaks

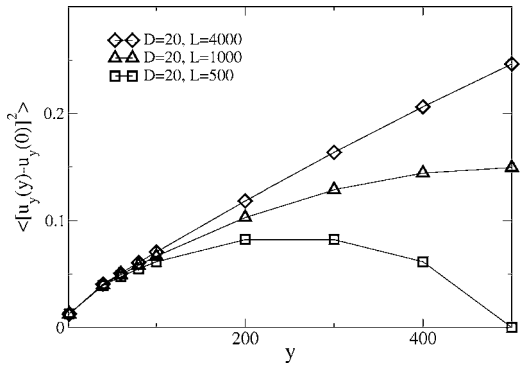

FIG. 16. Displacement correlation function $B(y)=\langle[u_y(y)-u_y(0)]^2\rangle$ plotted vs y, calculated according to Eqs. (19)–(21), for $L\times D$ systems with $D=20$ and $L=500$, 1000, and 2000, as indicated in the figure. Periodic boundary conditions are used in both x and y directions. As input parameters, the Lame coefficients $\lambda=42$, $\mu=41$, and the hydrostatic pressure $p=17.4$ (all these parameters are quoted in units of k_BT/σ^2) are taken, as obtained from the Monte Carlo simulation of the model, Eq. (47), at $T=1$ in the bulk. Note that $B(y)$ exhibits a symmetry $B(y)=B(L-y)$ due to the periodic boundary condition. $B(y)$ is given in units of σ^2 ($\sigma=1$).

down near the Kosterlitz-Thouless [25] transition (due to vortex pair formation the spin wave stiffness of the XY model gets renormalized), and similarly we expect that the agreement seen in Fig. 17 gets worse when the melting transition is approached: we expect that the elastic constants get renormalized due to dislocation-pair formation [27,35–39]. Although it would be very interesting to study our model at temperatures closer to the melting transition, we have not attempted to do this due to the enormous difficulties of obtaining well equilibrated simulation data. Already at $T=1$ for $y\geqslant 50$ Fig. 17 displays huge statistical errors, in spite of a run that lasted for many weeks at Pentium 4 or Xeon 2.66 Ghz processor. Therefore it is likely that there is no systematic discrepancy between the harmonic theory and the Monte Carlo results even for $y=L/2=250$. Anyway, one can see that for $y>40$ the increase of $B(y)$ with y is stronger than

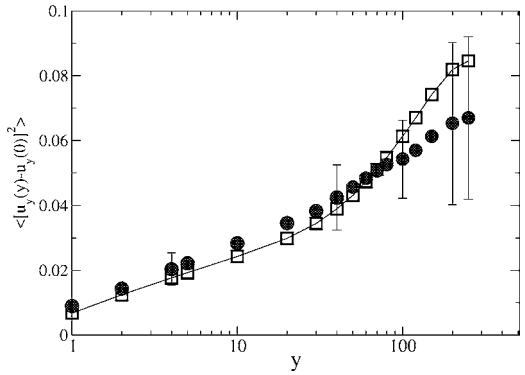

FIG. 17. Comparison of $B(y)$ according to the harmonic theory (Fig. 16), squares with corresponding Monte Carlo data (full dots with error bars), for a system with linear dimensions $D=20$, $L=500$, and periodic boundary conditions. Note the linear scale of the ordinate, while the abscissa is logarithmic. $B(y)$ is given in units of σ^2 ($\sigma=1$).

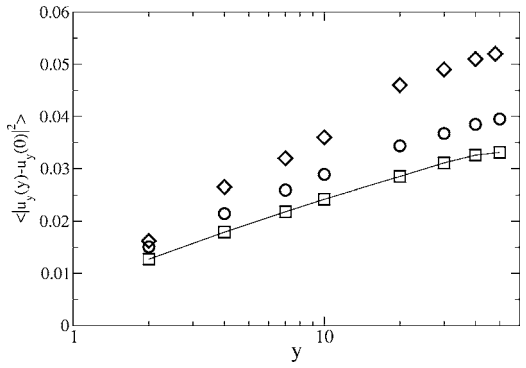

FIG. 18. Comparison of $B(y)$ according to the harmonic theory (squares) with corresponding Monte Carlo data (open circles), for a system with linear dimensions $D=20$, $L=100$, and periodic boundary conditions. The diamonds show corresponding Monte Carlo data for a system with planar walls, using only the displacement of particles in the rows adjacent to the walls. $B(y)$ is given in units of σ^2 ($\sigma=1$).

the initial logarithmic behavior. However, from Fig. 16 it is clear that the linear behavior according to Eq. (27) cannot really be seen, because the effects due to periodic boundary condition start rather early.

Figure 18 compares interesting results for the harmonic theory [Eqs. (19) and (20)] with Monte Carlo results for the case $D=20$, $L=100$, including also data for a system with planar walls, for the layers closest to the walls. In this case there seems to be some systematic discrepancy between the Monte Carlo data and the harmonic theory, but the general trend is similar. Having found above that the periodic boundary condition starts to be felt at $n\approx L/4$ already, no trace of an increase of $B(y)$ with y stronger than logarithmic is seen in this case. An interesting feature, however, is the faster increase of the displacement correlation function of particles adjacent to a hard wall, for a system of the same linear dimensions ($D=20$, $L=100$) but with two planar walls along the y axis rather than a periodic boundary condition. Unfortunately, the mild curvature of the data in Fig. 20 (due to the periodic boundary condition in the y direction, which is strongly felt for $y>L/4=25$) prevents us from making precise statements about the relation between the slope in the relations $B(y)\propto \ln y$ for a two-dimensional crystal surface adjacent to a flat wall and in the bulk, respectively. Recall that these prefactors are the analogs of the exponents $\eta_{\|}(T)$ and $\eta(T)$ in the XY model, respectively [cf. the discussion from Eq. (31) to Eq. (46)]. From Eq. (41) one would expect that the slope of the relation $B(y)\propto \ln y$ for a row adjacent to a wall is twice as large as the slope in the bulk.

Figurs 16–18 emphasize the aspect that a crystal in two dimensions is a critical system, as far as positional long range order is concerned. The instability of this order, evidenced by the growth of the displacement correlation function with distance, is enhanced by hard wall boundary conditions, similar to an XY model with free surfaces. This enhancement of fluctuations at the free surface (or hard wall, respectively) is felt over very large distances in the x direction, where also an anomalous enhancement of fluctuations exists [cf. Eq. (40)]. Presumably, these long range effects of

free surfaces are responsible for the difference between $C_{33}(n)$ for thin strips of n layers bounded by hard walls, and the corresponding systems with periodic boundary conditions in all directions.

V. STRIPS WITH WIDTHS THAT ARE INCOMMENSURATE WITH THE TRIANGULAR LATTICE STRUCTURE

In the previous sections, the strip width D was carefully chosen such that the ideal triangular lattice structure (e.g., with 30 rows) fits into the strip as perfectly as possible (recall Figs. 4 and 5, and accompanying discussion). Of course, it is also of interest to ask what happens when such a choice is not made, and D does not correspond to an integer multiple of the distance $a\sqrt{3}/2$ between rows in Fig. 2. Such questions have been considered in the literature (e.g., Refs. [6,11]) for ultrathin strips (containing a few rows only) and structures rather rich in defects (as compared to the ideal triangular lattice) were found. Here we ask the same question for a rather thick strip, and we shall show that the equilibrium states are elastically distorted (but otherwise defect-free) structures. However, varying D one can observe transitions in the number of rows ($n \to n \pm 1$) and these transitions are nucleated by the formation of dislocation pairs. Similar transitions in the number of layers or rows parallel to the bounding walls have also been observed for hard disk systems [9,10] in the canonical ensemble, as well as in a semi-grand-canonical study [85] where disks could be exchanged between the confined strip and a surrounding liquid bath. This points to the fact that such transitions are, in fact, ubiquitous and do not depend on the detailed nature of the system considered.

Thus we consider a geometry where in the y direction we maintain a linear dimension commensurate with the triangular lattice having a lattice spacing a, while in the x direction a misfit Δ is introduced,

$$L_x = D = \sqrt{3}a(n_x + \Delta)/2, \quad L_y = n_y a, \tag{56}$$

where in the following numerical examples we choose the integers $n_x=30$, $n_y=30$.

In principle, Δ can be any real number. We have found that for positive Δ (which implies a reduction of density in the system) one can observe a melting transition in the center of the strip, while the rows near the walls remain ordered (the situation is qualitatively analogous to the situation at higher temperatures in the commensurate case, cf. Figs. 6 and 7).

More interesting is the case of negative Δ, which means enhancement of the density since the number of particles in the rectangular box $L_x \times L_y$ is kept strictly fixed. For small $|\Delta|$ there is no change in the number of rows, but the lattice structure needs to deform (relative to the ideal triangular lattice in the bulk) to accommodate all the particles in the smaller area. Figure 19 shows the probability distribution of the order parameter $\Psi_{\vec{G}_0}$ [defined in Eq. (10)] for the case of structured walls.

Since due to the change of the angle α (Fig. 5) $\vec{G}_0$ is not a reciprocal lattice vector for the deformed lattice any more,

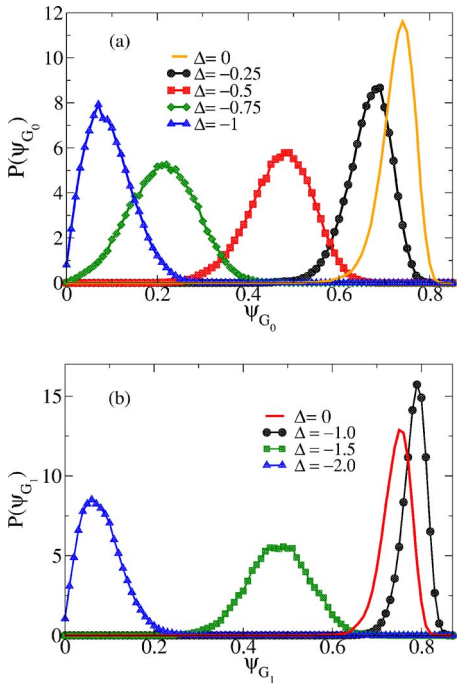

FIG. 19. (Color online) (a) Probability distribution of the order parameter $\Psi_{\vec{G}_0}$ in the case of structured walls for $n_x=n_y=30$, $T=1$ and several values of Δ as shown. (b) Same as (a) but for $\Psi_{\vec{G}_1}$.

we see that the larger $|\Delta|$ becomes the more $P(\Psi_{\vec{G}_0})$ gets shifted to the smaller values of $\Psi_{\vec{G}_0}$, as expected.

More interesting is the distribution of the order parameter $\Psi_{\vec{G}_1}$, since (Fig. 2) the reciprocal lattice vector $\vec{G}_1$ is directed along the x axis, orthogonal to the walls, and as long as we still have $n_x=30$ layers in the strip $P(\Psi_{\vec{G}_1})$ indicates a well-ordered system with a large value of $\Psi_{\vec{G}_1}$. In fact for $\Delta=-1$ the distribution is centered at a somewhat larger value than for $\Delta=0$, and the peak is clearly sharper: this happens because the compression of the strip in the x direction reduces the fluctuations in that direction, the particles are more confined in their rows. However, when Δ becomes negative enough, such as $\Delta=-1.5$, the situation changes, $P(\Psi_{\vec{G}_1})$ now is peaked near $\Psi_{\vec{G}_1} \approx 0.5$, and for $\Delta=-2.0$ the peak occurs near $\Psi_{\vec{G}_1} \approx 0.1$ [Fig. 19(b)]. The reason for this behavior is that a transition from $n=30$ to $n=29$ rows occurs, as is evident from Fig. 20(a). Note that in the upper part of the system shown in Fig. 20(a) one counts 30 rows, while in the central part there are only 29! For $\Delta=-2.0$, however, one has 29 rows throughout the system (although one dislocation pair necessarily is still present, since in 29 rows now containing 31 particles per row each one can accommodate only 899 rather than the total 900 particles, the extra particle causing a corresponding lattice defect [Fig. 20(c)]. While one can recognize that in the rows adjacent to the walls some of the particles seem to be well localized at the lattice positions, this is not the case for a number of particles whose positions seem to be smeared out along the y direction. This structure results from the fact that the wall atoms fixed at ideal lattice positions create a periodic potential with 30 potential wells in the present choice of linear dimensions, but 31 particles per row need to be accommodated. This does not happen by

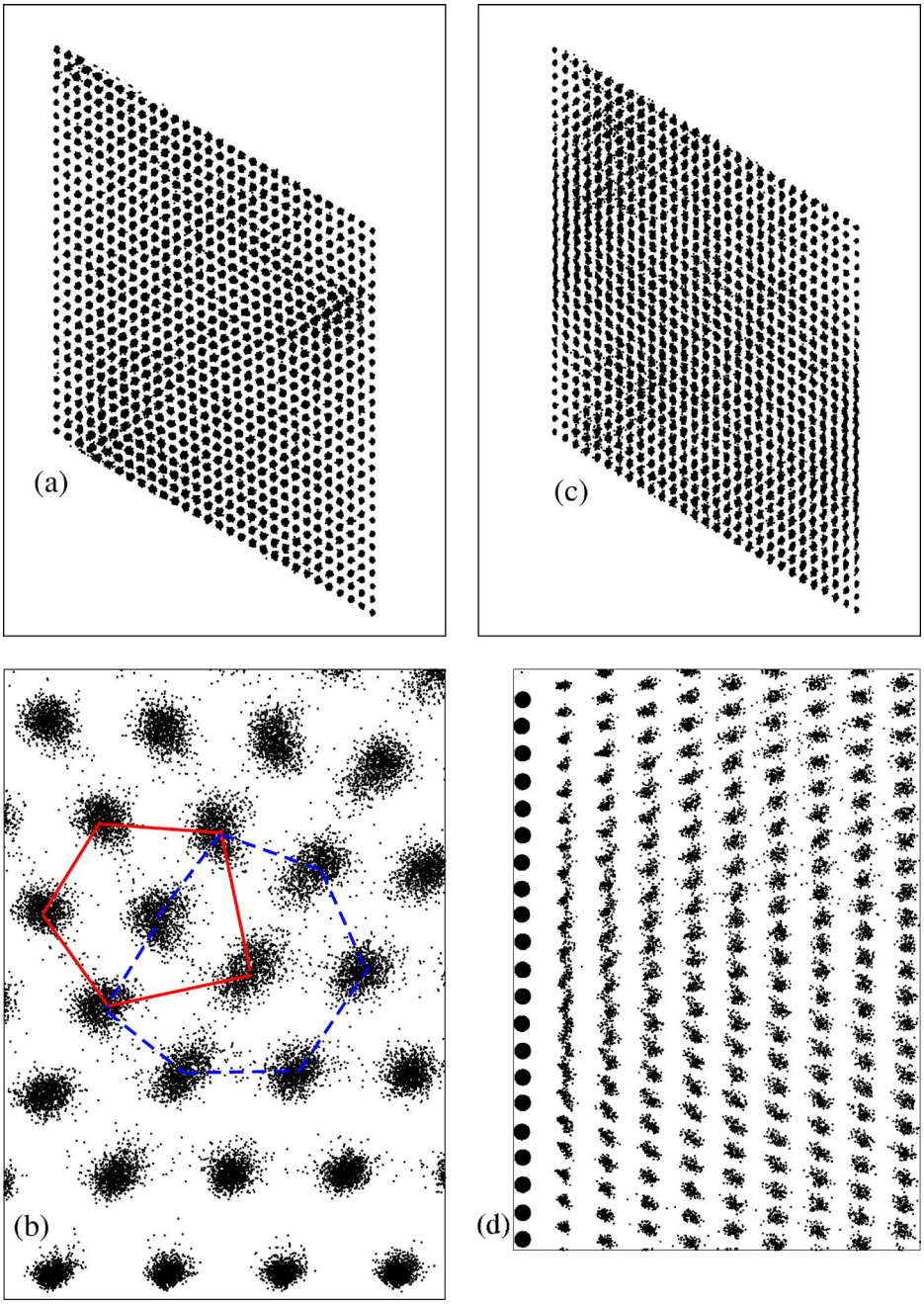

FIG. 20. (Color online) (a) Superimposed configurations in the case of a system with $n_x=n_y=30$, $T=1$, $\Delta=-1.5$, using the structured wall boundary condition. The top picture (a) shows the whole simulation box, while the middle part (b) shows a closeup of a dislocation pair, the sites with five or seven nearest neighbors, highlighted by full or broken lines, respectively. (c) Same as (a), but for $\Delta=-2.0$; 100 configurations are superimposed. (d) A close up near the wall of the figure in (c).

uniform compression of the distance between the particles, but rather this density enhancement is localized in a kind of solitonlike excitation which can diffuse along the row in the y direction, This interpretation is supported by a closeup of the structure [Fig. 20(d)], which also clearly shows that this defect of order in the first row propagates somewhat towards the interior rows of the strip. One can also recognize a slight bending of the rows.

It is also interesting to study the stress $\sigma=\sigma_{yy}-\sigma_{xx}$ [10], see Fig. 21, where σ is plotted as function of $|\Delta|$. In the regime of the critical linear increase, the stress is proportional to the geometrical strain $\tilde{\epsilon}$ measured with respect to the ideal bulk triangular lattice, $\tilde{\epsilon}=(a-a_x)/a=|\Delta|/n$, a_x being the lattice parameter corresponding to the reduced distance between rows in the x direction. After the initial increase we see a discontinuity at Δ_c (with about $|\Delta|=1.5$) where the system has started its internal structural rearrangement. Note, however, that for larger values of $|\Delta|$ the behavior is expected to be rather subtle: our structured wall boundary condition involves 30 particles per row, while—as discussed above—for $|\Delta|>|\Delta_c|$ the system has 31 particles per row in the y direction: so the "corrugation potential" provided by the walls is then incommensurate with the structure. In fact, with such an incommensurate wall potential we no longer expect any stabilizing effect on the positional long range order in the y direction in the system [19]. Also subtle finite size effects (associated with the finite size of $n_y=30$ atoms per row in the rows forming the wall potential) must be expected. A detailed study of these incommensurate structures for $|\Delta|>|\Delta_c|$ is beyond the scope of the present work,

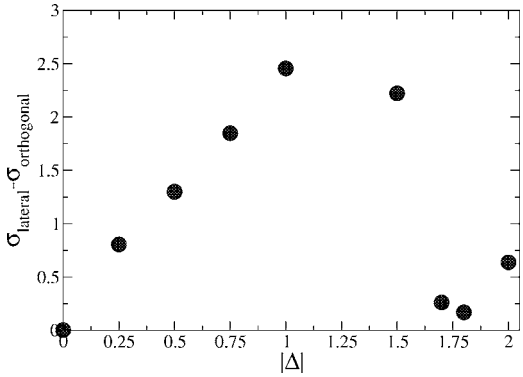

FIG. 21. Internal stress σ (in LJ units) inside the strip plotted vs $|\Delta|$, for the case $n_x=n_y=30$, $T=1$, and the structured wall boundary condition.

however, and must be left to future studies. We only note again that the superimposed snapshots for $|\Delta|=2$ [Figs. 20(c) and 20(d)], look much less ordered than their counterparts for $|\Delta|<|\Delta_c|$, due to these misfits between the system and its boundaries.

Also for the flat wall boundary condition the effect of varying Δ has been studied, and again a transition from $n_x=30$ to $n_x=29$ rows for sufficiently negative Δ was found. E.g., for $\Delta=-1.6$ even a bimodal distribution of $\Psi_{\vec{G}_1}$ was found [80]. A detailed analysis of these data revealed that the system stayed in the ordered state with $n_x=30$ rows for about 30 000 Monte Carlo steps (MCSs) per particle and then a rather sudden transition to a state with $n_x=29$ rows occurred, which remained stable for the remaining time of the run (up to 10^5 MCSs) [80]. While a detailed study of the kinetics of this phase transformation in such a simulation would be feasible, we are not presenting this here because the Monte Carlo method implies an artificial dynamics [82] which is not related to the actual dynamics of colloidal systems.

VI. CONCLUSION AND OUTLOOK

The effect of confining boundaries on the crystalline order of two-dimensional particles interacting with a pairwise repulsive potential was studied both by Monte Carlo simulations and by theoretical arguments, mostly based on the harmonic theory of crystal lattices. This study was motivated by possible experimental study of colloidal systems, which have proven to be an excellent model system for the experimental investigation of two-dimensional melting, and for which almost arbitrary boundary conditions can be created, for instance by strong laser fields. But also applications to a broad variety of other systems are conceivable (dusty plasmas, electrons at the surface of liquid helium, etc.), as discussed in the Introduction, and hence we did not "tailor" our model to simulate a particular real system as faithfully as possible, but rather we have concentrated on the generic aspects of the problem, and thus we have chosen a model which is computationally still relatively convenient, with an inverse power law (with a power $p=12$), and two types of confining boundaries, a structured wall (created by two rows of particles fixed in the positions of an ideal triangular lattice at the same density) and a flat planar wall (created by a repulsive potential of a strength tuned such that a minimal perturbation of the triangular crystal structure of the confined strip results).

The emphasis of our study has been to explore the consequences of the fact that even a bulk two-dimensional crystal is a critical system, which has only orientational long range order, while the positional long range order shows a power law decay of the appropriate correlation function (or, equivalently, the correlation of mean-square displacement shows a logarithmic increase with the distance between the particles). It was argued that the effect of confinement on such a system has several aspects: (i) due to the finite thickness D of a strip confined by two parallel boundaries a distance D apart, the system is quasi-one-dimensional (assuming that the other linear dimension L in the direction parallel to the walls is very large, ideally infinite). Already in a system with periodic boundary conditions in all directions, then a crossover occurs from the logarithmic increase of the mean-square displacement correlation to a linear increase with distance between the particles. This effect is even enhanced for a strip with flat planar boundaries, while for structured boundaries the crystalline order is stabilized, and the anomalous increase of the displacement correlation is suppressed.

Another consequence of confinement of two-dimensional crystals becomes apparent when one compares them to the analogous problem of surface effects on the two-dimensional XY ferromagnet. There the ferromagnetic long range order is absent, since (in the bulk) the displacement correlation $g(r)=\langle(\theta_0-\theta_r)^2\rangle$ between the angles θ of spins a distance r apart increases logarithmically, $g(r)=2\eta \ln r+\text{const}$, for large r, η being the well-known exponent describing the decay of the spin-spin correlation function, $\langle \vec{S}_0 \cdot \vec{S}_r \rangle \propto r^{-\eta}$. (Recall that $\langle \vec{S}_0 \cdot \vec{S}_r \rangle = \exp\left[-\frac{1}{2}\langle(\theta_0-\theta_r)^2\rangle\right]$ in the harmonic approximation that is considered here.) If both spins are at a free surface, this exponent is enhanced, $g_{\parallel}(r)=2\eta_{\parallel} \ln r+\text{const}$ with $\eta_{\parallel}=2\eta$, and also if one spin is at the surface and the other one deep in the bulk one also finds an enhancement, $g_{\perp}(x)=2\eta_{\perp} \ln x+\text{const}$, with $\eta_{\perp}=3\eta/2$. Similar enhancements of the displacement correlation functions in crystals are to be expected, too, if both (or one) of the considered sites lies next to the boundary. In fact, the numerical results (Fig. 18) are compatible with a relation $\eta_{\parallel}=2\eta$, although due to finite size effects it is not possible to generate a very strong evidence for this relation. The long range effect that a boundary has in the x direction perpendicular to the boundary is probably responsible for the anomalous behavior of the shear modulus of the strips confined by flat planar boundaries, which is vanishingly small (or at least an order of magnitude smaller than in the bulk). This apparent instability of the system against shear deformation in the y direction parallel to the boundaries implies that the system behaves like a two-dimensional smectic. Note that this instability (which we have found at a temperature $T=1$, in reduced units, while melting occurs at about $T_m \approx 1.35$) is not related to the formation of dislocations. We do find dislocation pair formation as a mechanism for transitions in the number of rows ($n_x \rightarrow n_x-1$) when we choose the strip thickness incommensurate with the proper triangular lattice structure at the chosen density, however. These transitions occur for both types of

boundary conditions, structured walls as well as flat planar walls. For the commensurate thickness of the strip, however, the structured wall suppresses the instability discussed above, and all elastic constants smoothly converge towards their bulk values as the strip thickness increases.

It also needs to be emphasized that the behavior studied in the present paper has nothing to do with surface-induced melting. In fact, a study of the system at $T > T_m$ rather shows evidence of surface-induced crystallization, since both types of boundaries cause a very strong layering effect in the x direction normal to the boundaries. This layering also implies that some residual orientational long range order is present at this strip at all temperatures. Moreover, it is shown that from an analysis of the decay of the surface-induced positional and orientational order one can extract information on the corresponding correlation lengths already in the fluid phase. Since these lengths strongly grow when the transition to the crystalline phase is approached, thin strips exhibit order already at temperatures above T_m. However, for a quantitative characterization of these lengths and their behavior near the transition substantially longer calculations for substantially larger systems than were possible in the present work would be required. The same statement applies to a study of a model with $p=3$ rather than $p=12$, which would correspond directly to the magnetic colloids used in many experimental studies.

Thus the present work is a first step only, and extensions in various directions are possible, including studies of dislocation formation and structure of incommensurate layers (Sec. V) near structured walls, and extensions to other crystalline structures. E.g., in binary colloidal systems also crystals with square lattice symmetry were detected [76], and a study of wall effects in these systems also would be interesting. Of course, also an extension to higher dimensionality (thin films rather than thin strips) is a very relevant problem. Surface instabilities, like the Raleigh instability in nanowires [86], which tend to break up a quasi-one-dimensional wire into beads of smaller length, are known to be stabilized by quantum effects. The instability discussed in this paper is different, but it also appears to degrade the properties a quasi-one-dimensional object by suppressing long range order. What is the role of quantum corrections to the kind of (bulk) instability discussed in this paper? We intend to report on some of these problems in future work.

ACKNOWLEDGMENTS

The present work received partial financial support from the Deutsche Forschungsgemeinschaft (DFG) under Grant No. TR6/C4. We are grateful to D. Chaudhuri, K. Franzrahe, and P. Henseler for useful discussions.

[1] W. C. Poon and P. N. Pusey, in *Observation, Prediction and Simulation of Phase Transitions in Complex Fluids*, edited by M. Baus, F. Rull, and J. P. Ryckaert (Kluwer, Dordrecht, 1995), p. 3; H. N. W. Lekkerkerker *et al.*, in *ibid.*, p. 53.
[2] T. Palberg, Curr. Opin. Colloid Interface Sci. **2**, 607 (1997).
[3] H. Löwen, J. Phys.: Condens. Matter **13**, R415 (2001).
[4] *Colloidal Dispersions in External Fields*, edited by H. Löwen and C. N. Likos, Special issue of J. Phys.: Condens. Matter **16**, No. 38 (2004).
[5] P. Glasson, V. Dotsenko, P. Fozooni, M. J. Lea, W. Bailey, G. Papageorgiou, S. E. Andresen, and A. Kristensen, Phys. Rev. Lett. **87**, 176802 (2001).
[6] G. Piacente, I. V. Schweigert, J. J. Betouras, and F. M. Peeters, Phys. Rev. B **69**, 045324 (2004).
[7] Y.-L. Lai and Lin I, Phys. Rev. E **64**, 015601(R) (2001); L. W. Teng, P. S. Tu, and Lin I, Phys. Rev. Lett. **90**, 245004 (2003).
[8] J. H. Chu and Lin I, Phys. Rev. Lett. **72**, 4009 (1994).
[9] P. Pieranski *et al.*, Mol. Phys. **40**, 225 (1980).
[10] D. Chaudhuri and S. Sengupta, Phys. Rev. Lett. **93**, 115702 (2004).
[11] R. Haghgooie and P. S. Doyle, Phys. Rev. E **70**, 061408 (2004).
[12] R. Haghgooie and P. S. Doyle, Phys. Rev. E **72**, 011405 (2005).
[13] K. Binder and P. C. Hohenberg, Phys. Rev. B **6**, 3461 (1972); **9**, 2194 (1974).
[14] K. Binder, in *Phase Transitions and Critical Phenomena*, Vol. 8, edited by C. Domb and J. L. Lebowitz (Academic, London, 1983), p. 1.
[15] H. W. Diehl, in *Phase Transitions and Critical Phenomena* (Ref. [14]), Vol. 10, p. 75.
[16] D. E. Sullivan and M. M. Telo da Gama, in *Fluid Interfacial Phenomena*, edited by C. A. Croxton (Wiley, New York, 1986), p. 45.
[17] S. Dietrich, in *Phase Transitions and Critical Phenomena* (Ref. [14]), Vol. 12, p. 1.
[18] G. Forgacs, R. Lipowsky, and T. M. Nieuwenhuizen, in *Phase Transitions and Critical Phenomena* (Ref. [14]), Vol. 14, p. 135.
[19] K. Binder, in *Cohesion and Structure of Surfaces*, edited by D. G. Pettifor (Elsevier, Amsterdam, 1995), p. 121.
[20] B. Berche, Phys. Lett. A **302**, 336 (2002).
[21] B. Berche, A. I. Farinas Sanchez, and V. Paredes, Europhys. Lett. **60**, 539 (2002).
[22] B. Berche, J. Phys. A **36**, 585 (2003).
[23] R. J. Baxter, *Exactly Solved Models in Statistical Mechanics* (Academic, London, 1982).
[24] M. E. Fisher, J. Phys. Soc. Jpn. **26**, 87 (1969).
[25] J. M. Kosterlitz and D. J. Thouless, J. Phys. C **6**, 1181 (1973).
[26] A. P. Young, in *Strongly Fluctuating Condensed Matter Systems*, edited by T. Riste (Plenum, New York, 1980), p. 271.
[27] D. R. Nelson, in *Phase Transitions and Critical Phenomena* (Ref. [14]), Vol. 7, p. 1.
[28] B. Nienhuis, in *Phase Transitions and Critical Phenomena* (Ref. [14]), Vol. 11, p. 1.
[29] J. L. Cardy, in *Phase Transitions and Critical Phenomena* (Ref. [14]), Vol. 11, p. 55.
[30] M. E. Fisher and V. Privman, Phys. Rev. B **32**, 447 (1985).

[31] V. J. Emery and J. D. Axe, Phys. Rev. Lett. **40**, 1507 (1978).
[32] J. D. Axe, in *Ordering in Strongly-Fluctuating Condensed Matter Systems*, edited by T. Riste (Plenum, New York, 1980), p. 399.
[33] P. M. Chaikin and T. C. Lubensky, *Principles of Condensed Matter Physics* (Cambridge University Press, Cambridge, England, 1995).
[34] N. D. Mermin, Phys. Rev. **176**, 250 (1968).
[35] B. I. Halperin and D. R. Nelson, Phys. Rev. Lett. **41**, 121 (1978).
[36] D. R. Nelson and B. I. Halperin, Phys. Rev. B **19**, 2457 (1979).
[37] A. P. Young, Phys. Rev. B **19**, 1855 (1979).
[38] K. J. Strandburg, Rev. Mod. Phys. **60**, 161 (1988).
[39] H. Kleinert, *Gauge Fields in Condensed Matter* (Singapore, World Scientific, 1989).
[40] Here the formula 3.7237 of I. S. Gradshteyn and I. M. Ryzhik, *Table of Integrals, Series and Products* (Academic, London, 1980), is used, $\int_{-\infty}^{+\infty}(x^2+c^2)^{-1}\{1-\cos[a(b-x)]\}dx = \pi[1-\exp(ac)\cos(ab)]/c$.
[41] B. Jancovici, Phys. Rev. Lett. **19**, 20 (1967).
[42] J. M. Kosterlitz, J. Phys. C **7**, 1046 (1974).
[43] H. W. J. Blöte and B. Nienhuis, J. Phys. A **22**, 1415 (1989).
[44] J. L. Cardy, Nucl. Phys. B **240**, 514 (1984).
[45] B. J. Alder and T. E. Wainwright, Phys. Rev. **127**, 359 (1962).
[46] W. G. Hoover and F. H. Ree, J. Chem. Phys. **49**, 3609 (1968).
[47] D. Frenkel and J. P. McTague, Phys. Rev. Lett. **42**, 1632 (1979).
[48] J. A. Zollweg, G. V. Chester, and P. W. Leung, Phys. Rev. B **39**, 9518 (1989).
[49] F. F. Abraham, Phys. Rev. Lett. **44**, 463 (1980).
[50] F. F. Abraham, in *Ordering in Two Dimensions*, edited by S. K. Sinha (North-Holland, Amsterdam, 1980), p. 155.
[51] J. Tobochnik and G. V. Chester, in *Ordering in Two Dimensions*, edited by S. K. Sinha (North-Holland, Amsterdam, 1980), p. 339.
[52] S. Toxvaerd, Phys. Rev. Lett. **44**, 1002 (1980).
[53] F. van Swol, L. V. Woodcock, and N. J. Cape, J. Chem. Phys. **73**, 913 (1980).
[54] J. A. Barker, D. Henderson, and F. F. Abraham, Physica A **106**, 226 (1981).
[55] J. Q. Broughton, G. H. Gilmer, and J. D. Weeks, Phys. Rev. B **25**, 4651 (1982).
[56] J. A. Zollweg and G. V. Chester, Phys. Rev. B **46**, 11186 (1992).
[57] J. Lee and K. J. Strandburg, Phys. Rev. B **46**, 11190 (1992).
[58] K. Naidoo, J. Schnitker, and J. D. Weeks, Mol. Phys. **80**, 1 (1993).
[59] K. Naidoo and J. Schnitker, J. Chem. Phys. **100**, 3114 (1994).
[60] H. Weber and D. Marx, Europhys. Lett. **27**, 593 (1994).
[61] H. Weber, D. Marx, and K. Binder, Phys. Rev. B **51**, 14636 (1995).
[62] A. Santos, M. Lopez de Haro, and S. Bravo Yuste, J. Chem. Phys. **103**, 4622 (1995).
[63] K. Chen, T. Kaplan, and M. Mostoller, Phys. Rev. Lett. **74**, 4019 (1995).
[64] K. Bagchi, H. C. Andersen, and W. Swope, Phys. Rev. E **53**, 3794 (1996).
[65] A. Jaster, Europhys. Lett. **42**, 277 (1999).
[66] A. Jaster, Phys. Rev. E **59**, 2594 (1999).
[67] S. Sengupta, P. Nielaba, and K. Binder, Phys. Rev. E **61**, 6294 (2000).
[68] K. Binder, S. Sengupta, and P. Nielaba, J. Phys.: Condens. Matter **14**, 2323 (2002).
[69] B. V. Derjaguin and L. D. Landau, Acta Physicochim. URSS **14**, 633 (1941).
[70] E. J. W. Verwey and J. Th. G. Overbeek, *Theory of the Stability of Lyophobic Colloids* (Elsevier, Amsterdam, 1948).
[71] K. Zahn, J. M. Mendez-Alcaraz, and G. Maret, Phys. Rev. Lett. **79**, 175 (1997).
[72] K. Zahn, R. Lenke, and G. Maret, Phys. Rev. Lett. **82**, 2721 (1999).
[73] K. Zahn and G. Maret, Phys. Rev. Lett. **85**, 3656 (2000).
[74] C. Eisenmann, P. Keim, U. Gasser, and G. Maret, J. Phys.: Condens. Matter **16**, S4095 (2004).
[75] J. P. Hansen and I. R. McDonald, *Theory of Simple Liquids* (Academic, London, 1986).
[76] P. Nielaba, K. Binder, D. Chaudhuri, K. Franzrahe, P. Henseler, M. Lohrer, A. Ricci, S. Sengupta, and W. Strepp, J. Phys.: Condens. Matter **16**, S4115 (2004).
[77] S. Sengupta, P. Nielaba, M. Rao, and K. Binder, Phys. Rev. E **61**, 1072 (2000).
[78] D. R. Squire, A. C. Holt, and W. G. Hoover, Physica (Amsterdam) **42**, 388 (1969).
[79] F. Varnik, J. Baschnagel, and K. Binder, J. Chem. Phys. **113**, 4444 (2000).
[80] A. Ricci, Ph.D. dissertation Johannes Gutenberg Universität Mainz, Mainz, Germany, 2006.
[81] K. Binder and D. W. Heermann, *Monte Carlo Simulation in Statistical Physics. An Introduction*, 4th ed. (Springer, Berlin, 2002).
[82] D. P. Landau and K. Binder, *A Guide to Monte Carlo Simulation in Statistical Physics*, 2nd ed. (Cambridge University Press, Cambridge, England, 2005).
[83] A brief account of these results has been presented earlier in A. Ricci, P. Nielaba, S. Sengupta and K. Binder, Phys. Rev. E **74**, 010404(R) (2006). Note, however, that $S(\mathrm{q})$ in the upper part of Fig. 1 of this communication is in error, it shows $S(\mathrm{q})$ for the structured wall at temperature $T=0$ rather than at $T=1$.
[84] P. Müller and A. Saul, Surf. Sci. Rep. **54**, 157 (2004).
[85] A. Chaudhuri, S. Sengupta, and M. Rao, Phys. Rev. Lett. **95**, 266103 (2005).
[86] C.-H. Zhang, F. Kassubek, and C. A. Stafford, Phys. Rev. B **68**, 165414 (2003).